LA-UR-85-1545

RECEIVED BY OSTI JUN 07 1985

CONF-850760 --1

LA-UR--85-1545

DE85 012689

TITLE: COSMOGENIC NEUTRON-CAPTURE-PRODUCED NUCLIDES IN STONY METEORITES.

AUTHOR(S): M. S. Spergel, York College of C.U.N.Y.

R. C. Reedy, Los Alamos National Laboratory

O. W. Lazareth, Brookhaven National Laboratory

P. W. Levy, Brookhaven National Laboratory

SUBMITTED TO: Proceedings of the 16th Lunar and Planetary Science Conference.

Los Alamos Los Alamos National Laboratory
Los Alamos, New Mexico 87545

Cosmogenic Neutron-Capture-Produced Nuclides in Stony Meteorites

M.S. Spergel

Department of Natural Science, York College of C.U.N.Y.

R. C. Reedy

Nuclear Chemistry Group, Los Alamos National Laboratory

O. W. Lazareth and P. W. Levy

Department of Physics, Brookhaven National Laboratory

Short title: Neutron-Capture Nuclides in Stony Meteorites

Abstract

The distribution of neutrons with energies below 15 MeV in spherical stony meteoroids are calculated using the ANISN neutron-transport code. The source distributions and intensities of neutrons are calculated using cross sections for the production of tritium. The meteoroid's radius and chemical composition strongly influence the total neutron flux and the neutron energy spectrum, while the location within a meteoroid only affects the relative neutron intensities. Meteoroids need to have radii of more than 50 g/cm^2 before they have appreciable fluxes of neutrons near thermal energies. Meteoroids with high hydrogen or low iron contents can thermalize neutrons better than chondrites. Rates for the production of ^{60}Co, ^{59}Ni, and ^{36}Cl are calculated with evaluated neutron-capture cross sections and neutron fluxes determined for carbonaceous chondrites with high hydrogen contents, L-chondrites, and aubrites. For most meteoroids with radii < 300 g/cm^2, the production rates of these neutron-capture nuclides increase monotonically with depth. The highest calculated ^{60}Co production rate in an ordinary chondrite is 375 atoms/(min g-Co) at the center of a meteoroid with a 250 g/cm^2 radius. The production rates calculated for spallogenic ^{60}Co and ^{59}Ni are greater than the neutron-capture rates for radii less than ~ 50-75 g/cm^2. Only for very large meteoroids and chlorine-rich samples is the neutron-capture production of ^{36}Cl important. The results of these calculations are compared with those of previous calculations and with measured activities in many meteorites.

Introduction

Meteorites, before they fall to the earth, are exposed to energetic cosmic-ray particles that induce nuclear reactions. To unfolding the cosmic-ray exposure history of a meteorite, it is best to use a variety of cosmogenic products such as tracks and nuclides with different production properties. Neutron-capture reactions, which vary considerably with depth and meteorite size (Eberhardt et al., 1963), are a good candidate for study. The neutron-capture production profiles are very different from those for tracks or from nuclides made by energetic cosmic-ray particles via spallation reactions. In large meteorites, neutron-capture reactions are the main source of several cosmic-ray-produced nuclides, such as ^{59}Ni and ^{60}Co (Eberhardt et al., 1963). Recently, the cosmogenic radionuclide ^{60}Co, produced by the $^{59}Co(n,\gamma)\ ^{60}Co$ reaction, has been very useful in unfolding the cosmic-ray exposure record of the large Jilin (Kirin) chondrite (Honda et al., 1982, Heusser and Ouyang, 1981).

Eberhardt et al. (1963) calculated the rates for the neutron-capture reactions producing ^{36}Cl, ^{59}Ni, and ^{60}Co in meteorites using neutron slowing-down theory. Lingenfelter et al. (1972) used neutron-transport theory to determine the fluxes of low-energy neutrons in the moon and in turn to calculate neutron-capture-induced isotopes in the moon. Recently we have used neutron-transport theory to calculate the low-energy neutrons flux as a function of depth in spherical meteoroids (Spergel et al., 1980a) and reported preliminary results for the production rates of ^{59}Ni and ^{60}Co (Spergel et al., 1981, 1982). This paper describes the complete neutron flux results and production rates for ^{36}Cl, ^{59}Ni, and ^{60}Co in stony meteoroids of various radii and compositions. Neutron-induced reactions in iron meteorites are also considered, but no estimates are made about

the production rates because of uncertainties in the neutron source functions. The relative neutron source strengths and neutron production-versus-depth profiles were determined using calculated ^{3}H production rates, and the absolute source strengths were normalized to that determined for the moon (Woolum et al., 1975). The energy spectrum of the source neutrons and the neutron-transport calculations using the ANISN computer code were similar to those used for the moon (Lingenfelter et al., 1972; Kornblum et al., 1973). The production rates of these three radionuclides as a function of depth in various spherical meteoroids were determined from the calculated equilibrium neutron-flux distributions and from energy-dependent neutron-capture cross section. Rates for producing these radionuclides by spallation reactions were also calculated.

The Theoretical Model

Neutron Source

The equilibrium flux of cosmogenic neutrons in a meteoroid (the meteorite before it was ablated while entering the earth's atmosphere) is determined from the source distribution of neutrons produced by cosmic-ray particles and the subsequent neutron transport. Neutron production rates in meteoroids could be calculated using both cross sections for neutron production and particle fluxes (Lingenfelter and Ramaty, 1967). However, neutron-production cross sections are not available for many of the source reactions that occur in meteorites. Because the excitation functions for producing neutrons are similar in shape to those for making tritium (Eberhardt et al., 1963; Lingenfelter and Ramaty, 1967), we used tritium (^{3}H) production rates to determine the relative neutron production rates in the moon and meteorites.

The excitation functions for the reactions making ^{3}H and the galactic-cosmic-ray (GCR) particle fluxes in the moon were those of Reedy and Arnold (1972). For meteoroids with radii from 20 to 2000 g/cm^2, the GCR particle fluxes were determined using spectral shapes and integral fluxes above 1 GeV calculated with the same equations and parameters as those used for the moon (Reedy and Arnold, 1972). The spectral-shape parameters used as a function of depth in meteoroids were determined by interpolating these parameters for the primary GCR particles, for the St. Severin chondrite (R = 70 g/cm^2) (Reedy et al., 1979), for the Jilin chondrite (R = 300 g/cm^2, obtained by fitting the measured ^{22}Na activities (Heusser and Ouyang, 1981)), and for the moon (Reedy and Arnold, 1972). These spectral-shape parameters and the calculated production rates for meteorites are discussed by Reedy (1985). The fluxes of primary GCR particles to which meteoroids were exposed were assumed to be 10% greater than those for the moon (Reedy et al., 1979). For both the moon and meteoroids, the ratios of measured/calculated ^{3}H activities were similar, about 1.4. The calculated ^{3}H production profiles for meteoroids of various radii were similar in trend to those of Trivedi and Goel (1973), but were $\sim$0.5 of their absolute values. The neutron production profiles monotonically increased with depth for meteoroids having R < 70 g/cm^2, and mainly decreased with depth for R > 300 g/cm^2. Compared to the ^{3}H production profile of Trivedi and Goel (1973), the ones calculated here increased less rapidly with depth near the surface and decreased slower with increasing depth for large radii.

Depth dependence of neutron source

The production profiles G(R,r) used for source neutrons for a given radius, R, and distance from the center, r, are shown in Figure 1. These were obtained by fitting the ^{3}H production profiles with

$$G(R,r) \propto (R-r+a)\cdot\exp(-(R-r)/L) \qquad (1a)$$

near the surface, where a = 125 g/cm^2, the approximate location of the peak neutron production is at r = R-(L-a), and with the function

$$G(R,r) \propto \exp(-R/L)\cdot\cosh(r/L) \qquad (1b)$$

at greater depths, L = 155 g/cm^2 being the "e-folding" length for source neutrons in the moon (Kornblum et al., 1973). These representations for the production profile were joined smoothly at an intermediate depth. The e-folding length adopted here (L = 155 g/cm^2) was determined from the experimental depth-versus-activity profiles for ^{37}Ar in the moon (Kornblum et al., 1973), and is slightly smaller than that (165 g/cm^2) used by Lingenfelter et al. (1972). Such a small difference in L should not be important for most applications as most meteorites had radii much less than L. Similar values corresponding to L were used by Eberhardt et al. (1963) for large meteorites, but varied with radius. For slab geometries (semi-infinite planes), like the moon, a pure exponential with L = 155 g/cm^2 was used (Kornblum et al., 1973). The ^{3}H production rate calculations suggest that, for a slab, a neutron source constant to about 30 g/cm^2 followed by the exponential might be more realistic, but transport calculations (Lingenfelter et al., 1972) showed that the equilibrium neutron fluxes were not very sensitive to such a small variation in the source term.

Absolute Neutron Source Intensity

The absolute intensity of the source neutrons in meteoroids also were determined from the calculated ^3H production rates. These production rates for the moon and meteoroids were integrated over all depths to get the total ^3H production rate. For meteoroids, these total rates were divided by the surface area (assuming a density of 3.5 g/cm^3) to get the rate per unit surface area. These ^3H production rates per unit surface area then were converted to absolute neutron source strengths per unit area by using the lunar neutron source strength of 12.8 neutrons/(cm^{2}s) determined by the Lunar Neutron Probe Experiment (Woolum et al., 1975). A very large meteoroid was assumed to have a source strength near 14.2 neutrons/(cm^{2}s), 10% greater than that for the moon (Reedy et al., 1979). These neutron source strengths for meteoroids of various radii are shown in Figure 2. The ^3H production rates of Trivedi and Goel (1973) also were integrated over depth and divided by surface area. For R < 100 g/cm^2, the shape of their integrated rates per area as a function of meteoroid radius were similar to that in Figure 2. However, when normalized to our results for R < 100 g/cm^2, their curve for R > 100 g/cm^2 dropped below ours, and was 0.46 of our result for an infinite radius. These deviations at large radii are due to large differences in the rate at which the ^3H production rates decreased with increasing depth. For depths of more than 100 g/cm^2, the e-folding lengths for ^3H production rates calculated here and by Trivedi and Goel (1973) were 148 and 74 g/cm^2, respectively. We believe that the shape in Figure 2 of the absolute neutron source strength versus meteoroid radius is determined well and that the absolute values obtained by normalization to the lunar source strengths are good.

Neutron Source Energy Dependence

The energy dependence of the neutron source is taken as a combination of evaporation and knock-on neutrons. The neutron source dependence is given of the form:

$$F(E) \propto \left[a \cdot E \exp(-E/T) + b \cdot \theta(3<E<10 \text{ MeV}) + c \cdot \theta(10<E<15 \text{ MeV})\right] \quad (2)$$

where θ represents step functions over the indicated "knock on" neutron energies; a, b and c are set to yield 62% of the neutrons as evaporation neutrons, 14% as the lower and 24% as the higher energy "knock on" neutrons (Kornblum et al., 1973). The evaporation neutrons are peaked at 1 MeV (T = 1 MeV). The complete neutron source, in units of neutron/g·s·eV, for a given size meteorite of radius R at an intermediate radius r ($r \leq R$).

$$S(R,E,r) = S_0(R)F(E)G(R,r) \quad (3)$$

where $S_0(R)$ is the absolute neutron source strength for a meteoroid of radius R and where the neutron's source dependence, G(R,r), and its energy dependence F(E) are normalized to unity.

Neutron Transport Model

The equilibrium flux of neutrons, $\phi(E,r)$, neutrons/($cm^2 \cdot s \cdot eV$), is calculated using the neutron transport techniques with multigroup theory (Lingenfelter et al., 1972) with eq. (3) as the source of neutrons. The neutron flux $\phi(E,r)$ is calculated for a one-dimensional spherical geometry as a function of radius, r, and neutron energy, (E), from the neutron transport equation after the manner suggested by Lingenfelter et al. (1972).

$$\mu \frac{\partial \phi_n}{\partial r}(r,\mu) + \sigma_n \phi_n(r,\mu) = \sum_{\ell} \frac{2\ell+1}{4\pi} P_\ell(\mu) \sum_g \phi_g^{(\ell)}(r) \sigma_{g \to n}^{(\ell)} + S_n(r) \quad (4)$$

where

μ = cosine of the angle with respect to increasing r;

$P_\ell(\mu)$ = Legendre polynominal of order "ℓ";

σ_n = macroscopic cross section for total energy group, n, of the bulk meteorite in cm^2/g;

$\sigma^{(\ell)}_{g\to n}$ = Legendre moment of the macroscopic scattering cross section from energy group "g" to energy group "n";

$S_n(r)$ = the energy source for the nth energy group (neutrons/g s);

$\phi_n(r,\mu)$ = the nth neutron energy group angular flux (neutrons/cm^2 s) within $d\mu$ of the μ direction;

$\phi^{(\ell)}_n(r)$ = the ℓth Legendre moment; and $\phi^{(o)}_n(r)$ is the group scaler flux, often referred to as the equilibrium flux of neutrons, (neutrons/cm^2 s), with energy between $E-\epsilon_n/2$ and $E+\epsilon_n/2$ (ϵ_n = width of the nth energy group) at depth d.

The neutron transport equation (eq. 4) is solved for spherical or slab geometries using the ANISN Code (Engle, Jr., 1967) which uses a discrete mesh in r and μ. The present calculation is a P1-S8 type indicating a P_1 Legendre polynomial expansion within eight angular quadratures. A radial interval size of about 2% of the meteorite's radius was found to give essentially the same results as finer intervals. The neutron energy interval or group structure used in ANISN is the GAM II structure (Joanou and Dudek, 1963) to take advantage of the extensive EPR-DLC37 (Plaster et al., 1975) tables of elemental neutron scattering cross sections. The GAM II energy structure (Joanou and Dudek, 1963) consists of 99 energy groups between 0.41 eV and 14.92 MeV and an additional single low energy (thermal) group for the energies from 1×10^{-5} to 0.41 eV. The use of a single ther-

mal group is adequate in cases, like ours, that investigate isotopes which do not have nuclear resonant behavior below 0.41 eV.

The discrete source term in equation (4) for a given size meteorite of radius R is derived from equation (3) by summing the neutron source S(R,E,r) over the nth energy group and ith radial interval:

$$S_n(R,r_i) = 4\pi \int_{(E_n - \epsilon_{n/2})}^{(E_n + \epsilon_n/2)} dE \int_{(r_i - \Delta)}^{(r_i + \Delta)} dr\, r^2 S(R,E,r) \qquad (5)$$

where Δ is the interval width.

The neutron scattering macroscopic cross section used in the calculation for a meteorite is formed by adding the products of the microscopic cross section (Plaster et al., 1975) and their atomic densities (see Table 1) in the meteorite. Adjustments are then made to the scattering cross sections in the single thermal group. The thermal cross sections in the cross section set are modified to make them correspond to a material at a temperature of 300 K. (The EPR cross sections are for materials at 800 K.) The details of this adjustment are derived and discussed in Spergel et al. (1980b).

Neutron Induced Isotopes

The production rate P(r) at radius r of a neutron-capture-produced nuclide is calculated by multiplying the derived equilibrium neutron flux, $\phi_g^0(r)$ by the appropriate neutron capture cross section and summing over energy groups for a given depth,

$$P(r) = \sum_g \phi_g^{(0)}(r) N\sigma_g(n,\gamma) \qquad (6)$$

where $N\sigma_g(n,\gamma)$ is the macroscopic neutron capture cross section for the gth group. These neutron radiative capture cross sections, in the GAM-II structure, are calculated directly from evaluated experimental data (Kinsey, 1979) sets by using energy group averaging in the NJOY-80 computer program (MacFarlane and Boicourt, 1975).

Results

The Influence of Meteorite Size on the Equilibrium Neutron Flux

Neutron energy spectra at a given depth. The strongest influence on the equilibrium neutron flux within a meteorite is the size of the meteorite. The intensity and shape of the neutron energy distribution are found to vary rapidly with meteorite size in small meteorites with radius less then 0.5 meter (150 g/cm^2 for stony meteorites and 300 g/cm^2 for iron meteorites). The neutron fluxes, as a function of neutron energy, near the surface in L-chondrites of various radii are shown in Figure 3. The result for the 10 g/cm^2 radius meteorite has an energy distribution for the neutrons along the lines of the original production spectrum of evaporation and knock-on neutrons. The deviation of the neutron flux energy spectrum from that of the production energy spectrum is in the build-up of lower energy neutrons. The presence of more mass in the meteorites increases the build up of low energy neutrons by multiple scattering. The results for larger chondrites ($R \geq 150$ g/cm^2) approaches the 1/E neutron energy distribution expected for an infinite, perfectly-scattering medium. The flux for the lunar soil calculated here and by other (Lingenfelter et al., 1972; Kornblum et al., 1973), also displays this 1/E dependence. The neutron scattering washes out the details introduced by the neutron production spectrum at all but the highest neutron energies (these high energy neutrons suffer infrequent scattering collisions).

The shape of the energy distribution for the equilibrium neutrons, however, varies little with location within a given meteorite. The energy spectra for neutrons immediately below the surface and in the center of a L chondrite meteorite with a radius of 50 g/cm^2 and of an aubrite (like Norton Country) with R = 250 g/cm^2 are shown in Figure 4. The insensitivity of the energy distribution to depth is attributed to the more energetic neutrons. The scattering cross sections of the meteoritic material for high-energy neutrons are small, consequently these neutrons have relatively large mean free paths in the meteorites. The high-energy neutrons are therefore distributed throughout the meteorite. These energetic neutrons are down-scattered to become low-energy neutrons, which have short mean free paths. The combination of long range high-energy neutrons and locally scattered low-energy neutrons leads to the calculated nearly depth independent energy spectrum for the equilibrium neutrons. Other effects which depend upon the distribution of the neutron energy, such as cosmogenic induced relative isotopic abundance (see below), will also be depth insensitive.

Variation of equilibrium neutrons with depth. The total neutron flux (the total number of secondary neutrons per cm^2 per sec) varies with depth. This is shown in Figure 5 for L-chondrites, an iron meteorite, and the Apollo 11 soil. In the smallest meteorites (radii less than $\sim$250 g/cm^2) the neutron flux is a very slowly increasing function with depth, while for larger meteorites the neutron flux peaks at depths of $\sim$150 g/cm^2 and then tails off exponentially. The ^{235}U(n,f) reaction, because of its large thermal cross section, is a good probe for low-energy neutron intensity. The shape of the lunar neutron flux calculated with the Apollo

11 elemental abundance (Figure 5) is in good agreement with the $^{235}U(n,f)$ results for the chemically similar Apollo 17 soil (Woolum et al., 1975).

The Effect of Elemental Abundances

Energy spectrum of neutrons. L-chondrites, H-chondrites, C3-chondrites, aubrites (which have low iron contents), and iron meteorites have been examined with radii between 10 and 2000 g/cm^2. Table 1 lists the elemental abundances in the various meteorites examined as taken from a compilation by Mason (1979). The neutron flux as a function of energy near the surface of the meteorite is displayed for 300 g/cm^2 radius in an L-chondrite (Figure 3), an aubrite (Norton County) (Figure 4), a C3 chondrite and an iron meteorite (Figure 6). The energy distributions of neutrons within L-chondrites and H-chondrites of the same size are almost identical. The neutrons in the stony meteorites of radius 300 g/cm^2 display the 1/E structure with spectral detail imposed at high energies by neutron absorption peaks or valleys in the major constituents of the meteorites, principally ^{16}O, ^{28}Si, ^{24}Mg, and ^{56}Fe. The neutron spectrum for the iron meteorite (Figure 6) reflects the iron's strong neutron absorption.

Neutron depth dependence. The depth dependence of the energy integrated neutron flux for an iron meteorite, L-chondrites with various radii and a lunar soil of Apollo 11 elemental abundance is seen in Figure 5. In the Apollo 11 soil, as with the L-chondrite, there is a peak in the neutron flux between 100-200 g/cm^2 in depth. Large values of the mean free path of the neutron in the material (or correspondingly small values of the macroscopic total neutron cross section for the material) dictate a position for a neutron flux peak deep beneath the surface. The neutron flux energy and depth dependence displayed in Figures 4-6 show, as is

suggested by eq. 4 above and by others (Lingenfelter et al., 1972; Spergel et al., 1980a; Kornblum et al., 1973), that the main features of the neutron flux depend upon the total macroscopic cross section (which is averaged over the material of the meteorite). This total macroscopic cross section is insensitive to a large variation in the relative elemental abundances (with the exception of hydrogen) in the meteorite.

The addition of hydrogen will radically change the neutron distribution (Lingenfelter et al., 1961; Lapides et al., 1980). The scattering by hydrogen rapidly degrades the energy of the neutron. The neutron flux in hydrated meteorites will peak closer to the surface and then fall off more rapidly with depth than the dry (hydrogen-free) meteorites. The effect of the presence of hydrogen, (seen for 300 g/cm^2 meteorites in Figure 7), is displayed by comparing the neutron depth dependence in a hydrogen-rich meteorite (a C3 meteorite) with that in dry meteorites (L chondrite and iron). In the C3 meteorite, the neutron flux peaks within the first 60 g/cm^2 while within the dry meteorites the neutron flux doesn't attain their peak values until 100-200 g/cm^2 beneath the surface.

Production Rates of ^{60}Co, ^{59}Ni and ^{36}Cl by Neutron-Capture Reactions

The technique for calculating rates for neutron-capture reactions were discussed in detail in the earlier sections of this paper. The equilibrium neutron flux, both depth and energy dependent, was determined with neutron transport theory. The production rates for ^{60}Co and ^{59}Ni were obtained using experimental energy dependent (n,γ) cross sections for ^{59}Co and ^{58}Ni, respectively. The elemental abundances for Co, Ni and Cl used in these calculations are given in Table 1, except for cobalt level in aubrite which was set at 14 ppm.

The calculation of the production rates for ^{36}Cl was somewhat limited by the available energy-dependent cross section data. Only data for naturally occurring chlorine is available in the ENDF (Kinsey, 1979) cross section library. However, the available thermal or low-energy neutron data for ^{35}Cl and ^{37}Cl indicate that the neutron capture cross section for ^{35}Cl is dominant within natural chlorine (since $\sigma_{n\gamma}(^{35}Cl)/\sigma_{n\gamma}(^{37}Cl) = 100.5$ (Kinsey, 1979)). It is reasonable to use the cross sections for the natural chloride to calculate the ^{36}Cl production rate. In meteorites larger than 100 g/cm^2 where thermal neutron capture is domirant, the ^{36}Cl production rate will, to within ~1%, be the total neutron capture rate for natural chlorine.

Cobalt-60 production. The calculated ^{60}Co production rates in stony meteorites with R < 50 g/cm^2 (mass < 40 kg), are below 1 atom/min g-Co. The highest ^{60}Co pro-duction rates are found within stony meteorites when the radius is about 250 g/cm^2 (1.4 m across). In meteorites of radius greater than 400 g/cm^2, the ^{60}Co production rate peaks at a depth of about 175 g/cm^2 in L-chondrites, 125 g/cm^2 in C3 chondrites and 190 g/cm^2 in aubrites. In Figure 8 the ^{60}Co production rates for C chondrites are seen converging to the calculated lunar soil values as the meteorite size is increased. The Apollo 11 lunar elemental abundance and a neutron production rate at 12.8 n/(cm^2/s) were used in calculating the lunar soil activity, the calculated ^{60}Co production rates for the Apollo 11 soil is in good agreement with the ^{60}Co results from lunar core (Wahlen et al., 1973). The calculated ^{60}Co production rates are shown in Figure 9 for ~70 g/cm^2 meteorites of C3, aubrite and L-chondrite (on a "per g Co" basis). The production peak is closest to the surface in the hydrogen-rich C3 meteorite.

Cobalt-Nickel ratios. The ^{59}Ni production rates shown in Figures 10 and 11 display many similar features to those of the ^{60}Co activity. The peak ^{59}Ni production rate in meteorites greater than 400 g/cm^2 occurs about 10 g/cm^2 deeper than the peak for ^{60}Co. However, the $^{59}Ni/^{60}Co$ ratio varies with meteorite size and elemental abundance. The variation in this ratio is seen in Figures 12 and 13. The $^{59}Ni/^{60}Co$ variation is linked to the neutron energy spectra, which varies with the size of the meteorite. Nuclear production rates are energy dependent, at low energies the ^{60}Co production rate is much larger than the ^{59}Ni production rate. Consequently, the resulting ^{60}Co activity will be more sensitive than ^{59}Ni to variation in the low energy neutron flux. In the previous sections, it was seen that the fraction of neutrons with low energies rapidly increases with meteorite size up to a radius of $\sim$300 g/cm^2 in an L-chondrite. The decrease of the $^{59}Ni/^{60}Co$ ratio with increasing meteorite size reflects this increase of low-energy neutrons. In the C3 chondrite, the neutron energy structure approaches the 1/E shape in meteorites as small as 30 g/cm^2. Consequently, the $^{59}Ni/^{60}Co$ ratio varies little with meteorite size for meteorites larger than 50 g/cm^2. In aubrites, the neutron flux also approaches a 1/E shape in relatively small meteorites, (here, a meteorite with R = 50 g/cm^2 has a considerable low-energy neutron flux). The $^{59}Ni/^{60}Co$ ratio in an aubrite correspondingly shows little dependence on meteorite size.

The value of the $^{59}Ni/^{60}Co$ ratio is nearly constant with depth in most meteorites. This effect was expected as the shape of the neutron flux energy spectrum, as discussed above, shows little variation with depth within a meteorite. The $^{59}Ni/^{60}Co$ ratio can be used in the stony meteorite to determine the size of the parent meteorite from meteorite

fragments, if the parent meteorite was less than 75 g/cm^2 in radius. If the parent meteorite was larger than 75 g/cm^2 in radius, a lower limit on the size of the parent meteorite from its fragment can be set. In C3 chondrite this not possible.

Chlorine production. The ^{36}Cl production rates, like those of the ^{59}Ni and ^{60}Co, increases with meteorite size, reaching a maximum activation in ordinary chondrites of size of about 300 g/cm^2 in radius (Figure 14). In larger meteorites, the ^{36}Cl production rate reaches a maximum at depths of 190 g/cm^2. The ^{59}Ni/^{36}Cl ratio (Figure 15), like the ^{59}Ni/^{60}Co ratio shows large variation with meteorite size but remains nearly constant within a given meteorite. The arguments for the ^{59}Ni/^{60}Co behavior apply directly to the ^{59}Ni/^{36}Cl results.

Spallogenic Production Rates for ^{60}Co, ^{59}Ni and ^{36}Cl

These radionuclides also can be made in meteorites by spallation reactions induced by GCR particles with E > 3 MeV. The production rates for these nuclides by such energetic reactions need to be known in interpreting the measured activities of these radionuclides because the rates for spallation reactions will be greater than the rates for the neutron-capture reactions in smaller meteorites. For ^{60}Co and ^{59}Ni production, the main spallogenic reactions are ^{60}Ni(n,p)^{60}Co and ^{60}Ni(n,2n)^{59}Ni, respectively. For ^{36}Cl, the main target elements are calcium and iron. The rates for these spallation reactions were calculated using GCR-particle fluxes and reaction cross sections. The GCR-particle fluxes were those used above to determine the neutron-source profiles and strengths. The cross sections for the important reactions and the calculated production rates are described for each of these three radionuclides in the following paragraphs.

Spallogenic cobalt-60 production. The cross sections used for the $^{60}Ni(n,p)^{60}Co$ reaction were based on experimental data up to 15 MeV (Garber and Kinsey, 1976) and estimated from similar reactions at higher energies. The peak cross section for ^{60}Co from natural nickel was 45 mb at 8 MeV. Measured cross sections for analogous reactions were used for the $^{62}Ni(n,p2n)^{60}Co$ reactions, the only other important source of spallogenic ^{60}Co. About 10-20% of the spallogenic production of ^{60}Co was calculated to have been from ^{62}Ni. The calculated ^{60}Co production rates by these spallation reactions with a nickel concentration of 1.2% ranged from 0.25 atoms/min kg near the surface of very small or very large meteorites to 1.2 atoms/min kg near the centers of meteorites with radii of 70-300 g/cm^2. Production of ^{60}Co by solar cosmic rays should be very small as there are few reactions for making ^{60}Co with these particles. An L-chondrite needs to have a radius of over 50 g/cm^2 before the rate for making ^{60}Co by neutron-capture reactions is greater than that by spallation reactions.

Spallogenic nickel-59 production. The cross sections assumed for the $^{60}Ni(n,2n)^{59}Ni$ reaction at low energies were those measured for the $^{59}Co(n,2n)^{58}Co$ reaction (Garber and Kinsey, 1976). Cross sections for the (n,xn) reactions with heavier Ni isotopes were included, but the contributions of heavier isotopes to ^{59}Ni production were small. The peak cross section for making ^{59}Ni from natural nickel was 200 mb at 17-20 MeV. The calculated ^{59}Ni production rates for a Ni content of 1.2% ranged from about 1.5 to a little over 4 atoms/min kg. A small amount of ^{59}Ni could be produced near a meteoroid's surface by solar cosmic rays via the $^{60}Ni(p,pn)^{59}Ni$ and $^{56}Fe(\alpha,n)^{59}Ni$ reactions. The approximate radius of an

L-chondrite with equal production by spallation and neutron-capture reactions is 75 g/cm^2.

Spallogenic chlorine-36 production. The cross sections for the production of ^{36}Cl from potassium and calcium were those of Reedy and Arnold (1972), with the latter changed slightly at 1 GeV to fit recent experimental cross sections (Dedieu, 1979). The cross sections used for Fe(p,x)^{36}Cl were similar to shape to those of ref. 11, but increased to match experimental cross sections (Dedieu, 1979; Regnier et al., 1977; Baros and Regnier, 1984). For meteoroids with R = 40-100 g/cm^2, the calculated ^{36}Cl production rates from iron were 14-19 atoms/min kg-Fe and those from calcium were 130-240 atoms/min kg-Ca. The ratios of the production rate from calcium to that from iron varied by more than a factor of two for R = 40-100 g/cm^2, being low near the surface and high in the center of large meteoroids. The net rates for spallogenic ^{36}Cl in L-chondrites ranged from 3 to 8 atoms/min kg and usually were 6-7 atoms/min kg, in fairly good agreement with measured ^{36}Cl activities in chondrites (Begemann et al., 1969; Honda and Arnold, 1964). Solar-cosmic-ray production of ^{36}Cl should be small (Reedy and Arnold, 1972). As noted by Eberhardt et al. (1963), the spallogenic production of ^{36}Cl dominates unless the meteoroid is very large, the chlorine content is high, or both.

Comparison with Previous Results

Our calculated results from neutron fluxes and for neutron-capture-produced radionuclides are generally in good agreement with earlier calculations and with measurements in extraterrestrial samples. The results of our slab calculations agree with the calculation of Lingenfelter et al. (1972) and of Kornblum et al. (1973) and with the lunar neutron measurements (Woolum et al., 1975). The absolute values and

activity-versus-depth profiles calculated for ^{60}Co in the moon agree with the measured activities of Wahlen et al. (1973). The calculated results for large spheres are converging to those for a slab, but there still are significant differences between the results for a slab and for a sphere with a radius of 1000 g/cm^2. The calculated neutron fluxes and nuclide production rates for small spheres are quite different from those for large objects.

Calculations of Eberhardt et al.

The results of our calculations for spherical ordinary chondrites can be compared directly with those of Eberhardt et al. (1963). Both sets of calculations gave results that are quite similar. However, there are some minor differences. At the surface of a meteoroid, their ^{60}Co production rates were near zero, while our largest rate at the surface is about 13 atoms/min/g-Co for radii between 300 and 600 g/cm^2. Their maximum ^{60}Co production rate is about 13% above our largest value, 375 atoms/min/g-Co. Most of this difference is due to the absolute neutron source strengths; their semi-infinite medium source strength was about 13% greater than ours. Their production-rate-versus-depth profiles are slightly different. Their profile for R = 150 cm (about 525 g/cm^2) decreases from the maximum rate to the rate at the center more slowly than does our profile for 600 g/cm^2, possibly because they used a larger value equivalent to L (Eq. 1) in their neutron source profile. We both calculate differences in the $^{60}Co/^{59}Ni$ production ratios with radius. However, Eberhardt et al. (1963) did not report the variation we found for the $^{36}Cl/^{59}Ni$ production ratio in smaller meteorites.

Cobalt-60 Measurements in Various Meteorites

Jilin results. Our calculated production rates are in good agreement with the many measured ^{60}Co activities and with the few measured ^{59}Ni or ^{36}Cl activities. The very large (10^4 kg) Jilin (Kirin) H5 chrondrite that fell in 1976 had a pre-atmospheric radius that is known to have been about 300 g/cm^2 (Heusser and Ouyang, 1981). Measured ^{60}Co specific activities in many samples of Jilin range from 53 to 260 dpm/kg (Honda et al., 1982; Heusser and Ouyang, 1981), or about 71 to 347 dpm/g-Co, using a Co abundance of 750 ppm (G. Heusser, priv. comm.). These activities agree very well with our calculated production rates for R = 300 g/cm^2 (13-345 atoms/min/g-Co), indicating that our absolute source strengths are probably accurate. The lowest measured ^{60}Co activity corresponds to a pre-atmospheric depth of about 20 g/cm^2.

Allende results. The range of ^{60}Co activities measured in the large (mass > 2000 kg or R > 175 g/cm^2) Allende C3 chondrite was 9 to 226 dpm/kg (Cressy, Jr., 1972; Evans et al., 1982; Mabuchi et al., 1975; Bourot-Denise and Pellas, 1982) (14-356 dpm/g-Co assuming a Co abundance of 635 ppm (Cressy, Jr., 1972)), with most values between 41 and 185 dpm/kg. Our calculated production rates for C3 chondrites with 100 ppm of hydrogen range from 15 to 240 dpm/g-Co. As most C3 chondrites probably have quite low H contents (Mason, 1979; Cressy, Jr., 1972), the ^{60}Co activities in Allende should also be compared with the calculated rates for dry L-chondrites, which range up to 375 atoms/min/g-Co. The depths inferred in Allende from measured track densities and ^{60}Co activities agree well (Bourot-Denise and Pellas, 1982). The agreement with the depths inferred from calculations using a dry L-chondrite composition is better than that

for the C3 chemistry with 2300 ppm hydrogen, indicating that the hydrogen content of Allende was probably quite low.

St. Severin results. The LL6 chondrite St. Severin (recovered mass of 272 kg) had ^{60}Co activities that ranged from 1.9 to 21 dpm/kg (Cressy, Jr., 1970; Marti et al., 1969) or about 4 to 49 dpm/g-Co. The highest ^{60}Co activity corresponds to that calculated for the center of a R = 100 g/cm^2 chondrite (mass of 350 kg), consistent with the pre-atmospheric mass inferred by Bhandari et al. (1980). Marti et al. (1969) deduced from their data that the pieces with ^{60}Co activities of ~4 and ~26 dpm/g-Co were from depths of 8 cm (28 g/cm^2) and "close to the surface," while such production rates calculated for a R = 100 g/cm^2 chondrite correspond to depths of about 8 and 38 g/cm^2, respectively. These differences in the inferred depths could be because the pre-atmospheric body of St. Severin was non-spherical and these two pieces came from the sharp tip and flat surface of an ellipsoid. Unfortunately, the unusual shapes of some meteoroids is a potential complication for making comparisons with our calculations, which are for spherical objects.

Other cobalt-60 results. Except for the C2 chondrite Murchison, which has ^{60}Co activities of 79±3 and 53±2 dpm/kg (Cressy, Jr., 1972; Evans et al., 1982), almost all other chondrites have ^{60}Co activities that are below about 25 dpm/g-Co (Honda and Arnold, 1964; Evans et al., 1982; Cressy, Jr., 1970; 1971; Mabuchi et al., 1968; Shedlovsky et al., 1967). A chondrite with a radius of 90 g/cm^2 (mass of 250 kg) would have a maximum ^{60}Co production rate of 25 atoms/min/g-Co, so most recent falls probably had pre-atmospheric masses less than 250 kg. The two meteorites identified by Evans et al. (1982) as being small because of their high ^{22}Ne/^{21}Ne ratios, Canon City and Kabo, had low ^{60}Co activities, 1.1 ± 0.7

and 2.1 ± 0.9 dpm/g-Co, respectively. Most of the measured ^{60}Co activities in ref. 31 were 2 dpm/g-Co or less, and the contribution of spallation reactions to the total ^{60}Co production is significant. The lowest activities or limits for ^{60}Co, about 1 dpm/g-Co, are consistent with the calculated rates for spallogenic ^{60}Co. The ^{60}Co activity, 0.32 ± 0.08 dpm/kg, measured in one sample from Lost City is very low and is near the lowest rates calculated for spallogenic ^{60}Co, possibly because it fell just after solar maximum.

Due to the modulation of the galactic cosmic rays over an 11-year solar cycle, the production rates of cosmogenic nuclides, and of neutrons, varies by a factor of 2.5-3.0 (Evans et al., 1982). However, because of its 5.27-year half-life, ^{60}Co is made over several solar cycles and its activity will vary much less. The maximum ^{60}Co activity was calculated to occur 2.3 years after the minimum of solar activity and to be only 10% above that averaged over a complete solar cycle.

Nickel-59 Results

There are few activities of ^{59}Ni reported for stony meteorites, in part because of the need to do chemical separations and low-level X ray counting. Most measured ^{59}Ni activities are between 9 and 13 dpm/kg (Honda and Arnold, 1964; Mabuchi et al., 1968, 1975; Marti et al., 1969; Shedlovsky et al., 1967), well within the calculated range for neutron-capture reactions and above the rates calculated for spallogenic reactions. Such activities correspond to pre-atmospheric radii of $\gtrsim$ 100 g/cm^2. Both ^{60}Co and ^{59}Ni were measured for almost all of these samples. The ratios of $^{59}Ni/^{60}Co$ activities (in dpm/kg) were near 1, the ratio calculated here for L-chondrites. As the elemental ratio Ni/Co in all chondrites is about 21, independent of type, the $^{59}Ni/^{60}Co$ activity ratio

should not vary with the class of the chondrite, but only with the size. For very small meteorites ($R < 50$ g/cm^2), the spallogenic production ratio of $^{59}Ni/^{60}Co$, about 4, will dominate. The highest $^{59}Ni/^{60}Co$ activity ratio was for Granes 1.6 ± 0.6 (Mabuchi et al., 1968). This relatively high ratio and the low activities of ^{59}Ni and ^{60}Co, 10.5 ± 1.5 and 6.4 ± 1.5 dpm/kg, respectively, are consistent with a pre-atmospheric radius as small as 80 g/cm^2. The $^{59}Ni/^{60}Co$ activity ratio for an Allende sample was 0.91 ± 0.11 (Mabuchi et al., 1975), much less than the ratio of 1.9 calculated for a C3 Chondrite with 2300 ppm hydrogen; further evidence that the hydrogen content of Allende was quite low.

Chlorine-36 Results

There are very few experimental checks for the rates calculated for neutron-capture-produced ^{36}Cl, as almost all of the measured ^{36}Cl activities in stony meteorites are near the range of the spallogenic production rates. A high ^{36}Cl activity of 54 ± 2 has been reported for piece N . 3529 of Allende (Mabuchi et al., 1975). The calculated spallogenic production rate of ^{36}Cl in Allende is 7 ± 1 dpm/kg. Allowing a larger uncertainty for the spallogenic rate, the observed neutron-capture rate for ^{36}Cl in this specimen is 47 ± 4 dpm/kg. Reported chlorine abundances for bulk Allende samples are 220 ppm (Mason, 1979) and 237 ppm (Dreibus et al., 1979), and eight chlorine analyses in C3 chondrites (Mason, 1979; Dreibus et al., 1979) ranged from 149 to 370 ppm, with an average of 253 ± 63 ppm. Adopting a Cl content of 230 ppm, the neutron-capture rate for ^{36}Cl in this sample is 204 ± 17 dpm/g-Cl, considerably greater than the rate of 120 dpm/g-Cl calculated from the ^{59}Ni and ^{60}Co activities. As noted above, the calculated and observed ratios of ^{59}Ni and ^{60}Co in this specimen agreed well. The measured $^{59}Ni/^{41}Ca$ ratio, 2.94 ± 0.70 (Mabuchi

et al., 1975) is below, but agrees with, within relatively large uncertainties, the ratio calculated with thermal-neutron-capture cross sections. Mabuchi et al. (1975) suggested that this part of Allende lost a surface layer of about 10 cm thick during $10-10^4$ years before its fall. The agreement we find for ^{60}Co, ^{59}Ni, and ^{41}Ca indicate that such a loss would have had to occur about 2×10^5 years ago. The correlation of excess ^{36}Ar made by the decay of neutron-capture-produced ^{36}Cl and of ^{60}Co in inclusions from four Allende specimens (Göbel et al., 1982) does not require such a loss of surface layer. The high ^{36}Cl content could be due to a high chlorine abundance (about 390 ppm). Such an abundance is above the range measured in C3 chondrites, but is possibly given the heterogeneity of chlorine in Allende, especially the high Cl content of the fine-grained inclusions (Göbel et al., 1982).

Discussion

Our calculations allow us to investigate in detail the effects of meteoroid radius and elemental abundance and of sample depth on the fluxes of low-energy neutrons and on the rates for neutron-capture reactions. The most important parameter is the size or radius of the pre-atmospheric body. In small meteoroids, few neutrons are made, many neutrons escape, and most neutrons have not had enough scattering reactions to be slowed to near-thermal energies. Thus rates for neutron-capture reactions are very low. As the meteoroids become larger, the neutron source is higher, fewer neutrons leak out, and more neutrons are "thermalized" and the neutron spectrum approaches a 1/E shape. The magnitudes of measured activities of (n,γ) products are useful in establishing pre-atmospheric sizes. For a given radius in most meteoroids, the neutron spectral shape does not vary significantly with depth, and so the ratio of the activities of two neu-

tron-capture products can be used to set limits or to determine pre-atmospheric dimensions.

In larger meteoroids, the transport and leakage of neutrons cause large variations in neutron fluxes and capture rate with depth. The shapes of the production rate -versus-depth profiles vary considerably with depth. For R < 300 g/cm^2, the production rates increase monotonically from the surface to the center. For larger radii the production rates peak near a depth of 180 g/cm^2 and decrease toward both the surface and the center. The highest calculated ^{60}Co production rate in an ordinary chondrite is 375 atoms/min/g-Co near the center of a spherical meteoroid with a radius of about 250 g/cm^2.

The chemical composition of a meteoroid also influences the neutron spectrum and rates for neutron-capture reactions. The presence of hydrogen causes neutrons to be slowed rapidly and so hydrogen can considerably change the neutron fluxes and neutron-capture profiles in a meteoroid. The calculations for ordinary chondrites and C3 carbonaceous chondrites with water illustrate the influence of hydrogen on the neutron flux profiles in meteorites. The abundances of the elements in a meteorite together with their microsocopic cross sections will determine the neutron macroscopic cross section. The neutron transport is affected by the total macroscopic cross section. The calculations for ordinary chondrites should apply will to all dry (low hydrogen content) stony objects with similar macroscopic cross sections. The capture rate per target atom increases when the macroscopic cross section decreases (Reedy, 1978).

The large variation as a function of size and depth in the production rates of neutron-capture-produced nuclides make such products very useful in studies of the cosmic-ray exposure histories of meteorites. The

range of neutron-capture rates are much greater than that for the rates of producing nuclides via spallation reactions. In both Jilin (Honda et al., 1982; Heusser and Ouyang, 1981) and Allende (Cressy, Jr., 1972), the measured ^{60}Co activities varied by factors of 5 and 10, respectively, while the ^{22}Na and ^{26}Al activities change by less than a factor of two, and only exhibited a weak trend with the depths inferred from the ^{60}Co activities. The variation in the production rates of spallogenic nuclides with meteoroid radius is calculated to be much less than that for neutron-capture products. A few activities or isotopic ratios (e.g., $^{22}Ne/^{21}Ne$) of spallogenic nuclides do vary enough with depth or radius that they can be used in studies of depth effects in meteorites. Nuclear tracks are observed near the surfaces of meteorites and the track densities vary considerably with depth. All of these types of cosmic-ray records complement each other and together are powerful tools in unfolding the exposure histories of meteoritic samples. The large dynamic range of the rates for neutron-capture reactions are especially useful in studies of large meteorites.

Other products made by neutron-capture or similar reactions in meteorites should follow trends with radius, depth or chemistry that are similar to those calculated here for ^{60}Co, ^{59}Ni and ^{36}Cl. The stable decay products of ^{36}Cl, ^{36}Ar, can be readily measured (Göbel et al., 1982) and used as a record of a meteorite's integral exposure to cosmic rays. Neutron capture reactions with halogens also produced ^{80}Kr, ^{82}Kr, and ^{128}Xe in Allende inclusions (Göbel et al., 1982). Other radioactive nuclides made by (n,γ) reactions and occasionally measured in meteorites (Mabuchi et al., 1968, 1975) include ^{41}Ca and ^{45}Ca. In large objects with much nitrogen, ^{14}C would be made by thermal and epithermal neutrons via the

$^{14}N(n,p)^{14}C$ reaction. Many stable isotopic effects are produced by (n,γ) reactions (Lingenfelter et al., 1972), such as ^{158}Gd, and should be observable in large meteorites with long exposure ages (e.g., Norton County). Noble gases, other nuclides, and fission tracks can be produced by the fission of ^{235}U induced by low-energy neutrons, although in most meteorites cosmogenic fission will be dominated by energetic neutrons (E > MeV) reacting with ^{232}Th or ^{238}U. All of the reactions induced by thermal or epithermal neutrons should follow trends similar to those reported here.

The transport calculations reported here were for neutrons produced by galactic-cosmic-ray (GCR) particles. However, these basic trends for the transported neutrons as a function of radius, depth and chemistry would apply to neutrons produced by any type of energetic particles. In small spacecraft, neutron-capture reactions should be unimportant if the hydrogen content is low. Energetic solar ("SCR") particles can produce neutrons in the outer few centimeters of extraterrestrial objects, although the total number of SCR-produced neutrons are usually much less than those made by GCR particles. Our calculations show that the source neutrons have deep penetration into an object, controlling the spatial distribution of effects due to low-energy neutrons. The importance of SCR-particles in producing neutron-capture products should be small, even for most short-lived radionuclides immediately after a large solar flare.

In meteorites, many isotopic anomalies have been identified that apparently were produced near the time that the solar system was formed. Our calculations show that in order for neutron-capture products to be presently observable, a meteorite sample must have been part of an object whose preatmospheric size was greater than 50 g/cm^2 and also must have been situated at depths less than a few thousand g/cm^2 within the object.

A similar range of depths and radii also would apply to neutron-capture reactions induced by energetic particles at any time in the history of a piece of matter. The wide range of fluxes and capture rates calculated for low-energy neutrons in meteoroids would imply that any effects due to similar reactions in the early solar system also would vary considerably with sample location inside a extraterrestrial object.

Acknowledgments

We would like to acknowledge the efforts of Len Slatest and H rold Berry of the Applied Mathematics Department of BNL for his valuable assistance in calculating the (n,γ) cross sections and Mrs. Marilyn McKeown of the Physics Department of BNL for her general computing advice and guidance. The work performed at BNL was supported by the Division of Materials Sciences, U.S. Department of Energy, under contract DE-AC02-76CH00016. This work was also supported in part by NASA:W-14,084 and NASA:N[illegible] 7454. One of the authors (R.C.R.) thanks Professors F. Begemann and L. Schultz for their hospitality and the Max-Planck Gesellschaft for partial support during his stay at the Max-Planck-Institut für Chemie, Mainz, Fed. Rep. of Germany.

References

Baros, F. and S. Regnier, Measurement of cross sections for ^{22}Na, $^{20-22}Ne$ and $^{36-42}Ar$ in the spallation of Mg, Al, Si, Ca, and Fe. Production ratios of some cosmogenic nuclides in meteorites, J. Phys. (Paris), 45, 855-861, 1984.

Begemann, F., R. Rieder, E. Vilcsek, and H. Wänke, Cosmic-ray produced radionuclides in the Barwell and Saint-Severin meteorites, in Meteorite Research, P. M. Millman, ed., pp. 267-274, Reidel, Dordrecht, Holland, 1969.

Bhandari, N., D. Lal, R. S. Rajan, J. R. Arnold, K. Marti and C. B. Moore, Atmospheric ablation in meteorites: A study based on cosmic ray tracks and neon isotopes, Nucl. Tracks, 4, 213-262, 1980.

Bourot-Denise, M., and P. Pellas, Cosmic ray track densities and ^{60}Co activities as depth monitors in Allende meteoroid, Meteoritics, 17, 186, 1982.

Cressy, P. J., Jr., Multiparameter analysis of gamma radiation from the Barwell, St. Severin and Tatlich meteorites, Geochim. Cosmochim. Acta, 34, 771-779, 1970.

Cressy, P. J., Jr., Cosmogenic radionuclides in the Lost City and Ucera meteorites, J. Geophys. Res., 76, 4072-4075, 1971.

Cressy, P. J., Jr., Cosmogenic radionuclides in the Allende and Murchison carbonaceous chondrites, J. Geophys. Res., 77, 4905-4911, 1972.

Dedieu, J., Masures de sections efficaces de production d'isotopes de longue periode et leur interet astrophysique, thesis, University of Bordeaux, 1979.

Dreibus, G., B. Spettel, and H. Wänke, Halogens in meteorites and their primordial abundances, Phys. Chem. Earth, 11, 33-38, 1979.

Eberhardt, P., J. Geiss, and M. Lutz, Neutrons in meteorites, in Earth Science and Meteoritics, J. Geiss and E. D. Goldberg, eds., pp. 143-168, North-Holland, Amsterdam, 1963.

Engle, W. W., Jr., ANISN--A one-dimensional discrete ordinate transport code with anisotropic scattering, Union Carbide Corp., Computing Technology Center Report K1693, 1967.

Evans, J. C., J. H. Reeves, L. A. Rancitelli, and D. D. Bogard, Cosmogenic nuclides in recently fallen meteorites: Evidence for galactic cosmic ray variations during the period 1967-1978, J. Geophys. Res., 87, 5577-5591, 1982.

Garber, D. I., and R. R. Kinsey, Neutron cross sections; Volume II, curves, ERDA report number BNL-325, Third Edition, Volume II, 1976.

Göbel, R., F. Begemann, and U. Ott, On neutron-induced and other noble gases in Allende inclusions, Geochim. Cosmochim. Acta, 46, 1777-1792, 1982.

Heusser, G., and Z. Ouyang, Kirin, its irradiation ages and the reconstruction of its preatmospheric size, Meteoritics, 16, 326-327, 1981.

Honda, M., and J. R. Arnold, Effects of cosmic rays on meteorites, Science 143, 203-212, 1964.

Honda, M., K. Nishiizumi, M. Imamura, N. Takaoka, O. Nitoh, K. Horie, and K. Komura, Cosmogenic nuclides in the Kirin chondrite, Earth Planet. Sci. Lett., 57, 101-109, 1982.

Joanou, G. D., and J. S. Dudek, GAMII--A B_3 code for the calculation of fast neutron spectra and associated multigroup constants, General Atomic Report GA-4265, September 16, 1963.

Kinsey, R., Data formats and procedures for the evaluated nuclear data file ENDF, Brookhaven National Laboratory Report BNL-NCS-50496, 2nd edition, 1979.

Kornblum, J. J., E. L. Fireman, M. Levine, and A. Aronson, Neutrons in the moon, Proc. Lunar Sci. Conf., 4th, 2171-2182, 1973.

Lapides, J. R., M. S. Spergel, O. W. Lazareth, P. W. Levy, R. C. Reedy, and J. I. Trombka, The effects of hydrogen on gamma-ray emission from planetary surfaces, Lunar and Planetary Science XI, pp. 605-607, The Lunar and Planetary Institute, Houston, 1980.

Lingenfelter, R. E., and R. Ramaty, High-energy nuclear reactions in solar flares, in High-Energy Nuclear Reactions in Astrophysics, B. S. P. Shen, ed., pp. 99-158, W. A. Benjamin, New York, 1967.

Lingenfelter, R. E., E. H. Canfield, and W. N. Hess, The lunar neutron flux, J. Geophys. Res., 66, 2665-2671, 1961.

Lingenfelter, R. E., E. H. Canfield, and V. E. Hampel, The lunar neutron flux revisited, Earth Planet. Sci. Lett., 16, 355-369, 1972.

Mabuchi, H., J. Tobailem, C. Leger, R. Bibron, and D. Biettmann, Radioactivite induite par le rayonnement cosmique dans la meteorite Granes, Geochim. Cosmochim. Acta, 32, 949-963, 1968.

Mabuchi, H., Y. Nakamura, H. Takahashi, M. Imamura, Y. Yokoyama, and J. L. Reyss, Cosmogenic radionuclides in the Allende meteorite, Meteoritics, 10, 449, 1975.

MacFarlane R. E., and R. M. Boicourt, NJOY: A neutron and photon cross section processing system, Trans. Am. Nucl. Soc., 22, 720, 1975.

Marti, K., J. P. Shedlovsky, R. M. Lindstrom, J. R. Arnold, and N. G. Bhandari, Cosmic-ray produced radionuclides and rare gases near the surface of Saint-Severin meteorite, in Meteorite Research, P. M. Millman, ed., pp. 246-266, Reidel, Dordrecht, Holland, 1969.

Mason, B., Data of Geochemistry, Sixth edition; Chapter B. Cosmochemistry; Part 1. Meteorites, U. S. Geological Survey Professional Paper 440-B-1, 1979.

Mason, B., Table of C3 meteorites, Handbook of Elemental Abundances in Meteorites, Gordon, 1971.

Plaster, D. M., R. T. Santoro, and W. E. Ford III, Coupled 100-group neutron and 21-group gamma ray cross sections for EPR calculations, ORNL-TM-4872, April 1975, available from the Radiation Shielding Information Center of ORNL, as DLC-37.

Reedy, R. C., Planetary gamma-ray spectroscopy, Proc. Lunar Planet. Sci. Conf. 9th, pp. 2961-2984, 1978.

Reedy, R. C., A model for GCR-particle fluxes in stony meteorites and production rates of cosmogenic nuclides, J. Geophys. Res., 90, C722-728, 1985.

Reedy, R. C., and J. R. Arnold, Interaction of solar and galactic cosmic ray particle with the moon, J. Geophys. Res., 77, 537-555, 1972.

Reedy, R. C., G. F. Herzog, and E. K. Jessberger, The reaction Mg(n,α)Ne at 14.1 and 14.7 MeV: cross sections and implications for meteorites, Earth Planet. Sci. Lett., 44, 341-348, 1979.

Regnier, S., M. Baklouti, M. Simonoff-Lagarde, and G. N. Simonoff, Production of ^{36}Cl by high energy spallation, Phys. Lett., 68B, 202-204, 1977; with errata in F. Baros and S. Regnier, 1984.

Shedlovsky, J. P., P. J. Cressy, Jr., and T. P. Kohman, Cosmogenic radioactivities in the Peace River and Harleton chondrites, J. Geophys. Res., 72, 5051-5058, 1967.

Spergel, M. S., O. W. Lazareth, L. A. Slatest, and P. W. Levy, Energy averaged neutron cross sections for rock forming elements at astrophysically interesting temperatures, Lunar and Planetary Science XI, p. 1069, The Lunar and Planetary Institute, Houston, 1980b.

Spergel, M. S., R. C. Reedy, O. W. Lazareth and P. W. Levy, Depth dependence of cosmogenic nuclei in spherical meteoroids, Meteoritics, 15, 370, 1980a.

Spergel, M. S., R. C. Reedy, O. W. Lazareth, and P. W. Levy, Neutron capture reactions in meteorites, Meteoritics, 16, 387-388, 1981.

Spergel, M. S., R. C. Reedy, O. W. Lazareth, and P. W. Levy, Cosmic ray produced cobalt 60 in chondrites, Lunar and Planetary Science XIII, pp. 756-757, The Lunar and Planetary Institute, Houston, 1982.

Trivedi, B. M. P., and P. S. Goel, Nuclide production rates in stony meteorites and lunar samples by galactic cosmic radiation, J. Geophys. Res., 78, 4885-4900, 1973.

Wahlen, M., R. C. Finkel, M. Imamura, C. P. Kohl, and J. R. Arnold, ^{60}Co in lunar samples, Earth Planet. Sci. Lett., 19, 315-320, 1973.

Woolum, D. S., D. S. Burnett, M. Furst, and J. R. Weiss, Measurement of the lunar neutron density profile, The Moon, 12, 231-250, 1975.

M.S. Spergel
York College of CUNY
Jamaica, NY 11451
Brookhaven National Laboratory
Upton, NY 11973

R.C. Reedy
Los Alamos National Laboratory
Los Alamos, NM 87545

O.W. Lazareth and P.W. Levy
Brookhaven National Laboratory
Upton, NY 11973

Table 1. Elemental Abundances in Percent (Mason, 1979) of Meteorites

Elemental Composition	L-Chondrite	H-Chondrite	C3 Chondrite	Aubrite
Hydrogen	-	-	0.23[a]	0.04
Carbon	-	-	0.5	-
Oxygen	36.96	33.59	36.20	46.7
Sodium	0.65	0.58	0.38	0.10
Magnesium	15.2	14.2	14.5	24.6
Aluminum	1.1	1.01	1.33	0.32
Silicon	18.7	17.1	15.6	25.4
Phosphorus	0.10	0.11	0.16	0.01
Sulfur	2.15	2.0	2.3	0.50
Potassium	0.09	0.09	0.03	0.03
Calcium	1.3	1.2	1.8	0.47
Titanium	0.07	0.06	0.6	0.04
Chromium	0.38	0.34	0.35	0.05
Manganese	0.24	0.23	0.15	0.12
Iron	21.8	27.6	24.5	1.6
Cobalt	0.06	0.09	0.06	-
Nickel	1.2	1.8	1.3	0.04

[a]Assumed H content, as per Mason, 1971.

Table of Figures

Fig. 10. Nickel-59 production rates as a function of depth in L-chondrites with radii of 75, 150, 300, 600 and 1000 g/cm^2 and the lunar-Apollo 11 soil (Ni abundance taken at 1.2%).

Fig. 11. Nickel-59 production rates as a function of depth in a 300 g/cm^2 meteorites with compositions of L-chondrite, C3 and aubrite (given in per gram Ni present).

Fig. 12. Production ratios of $^{59}Ni/^{60}Co$ as a function of depth for L-chondrite meteorites with radii 75, 100, 150, 300, 600 and 1000 g/cm^2 and the lunar-Apollo 11 soil (^{59}Co abundance at 570 ppm and Ni at 1.3% by wt.).

Fig. 13. Production ratios of $^{59}Ni/^{60}Co$ in meteorites with a 300 g/cm^2 radius: L-chondrite (abundances taken: 570 ppm- Co; 1.27%- Ni), of C3 chondrite (abundances taken: 620 ppm- Co; 1.33%- Ni) and of aubrite (abundance taken: 14 ppm- Co; 200 ppm- Ni).

Fig. 14. Chlorine-36 production rates as a function of depth in 300 g/cm^2 meteorites with compositions of L-chondrite, C3, and aubrite (given in per gram of chlorine present).

Fig. 15. Production ratios of $^{59}Ni/^{36}Cl$ in meteorites with a 300 g/cm^2 radius: L-chondrite (abundances taken: 1.27%- Ni; 25 ppm chlorine), of C3 chondrite (abundances taken: 1.33%- Ni; 25 ppm chlorine) and of aubrite (abundances taken: 200 ppm- Ni; 25 ppm chlorine).

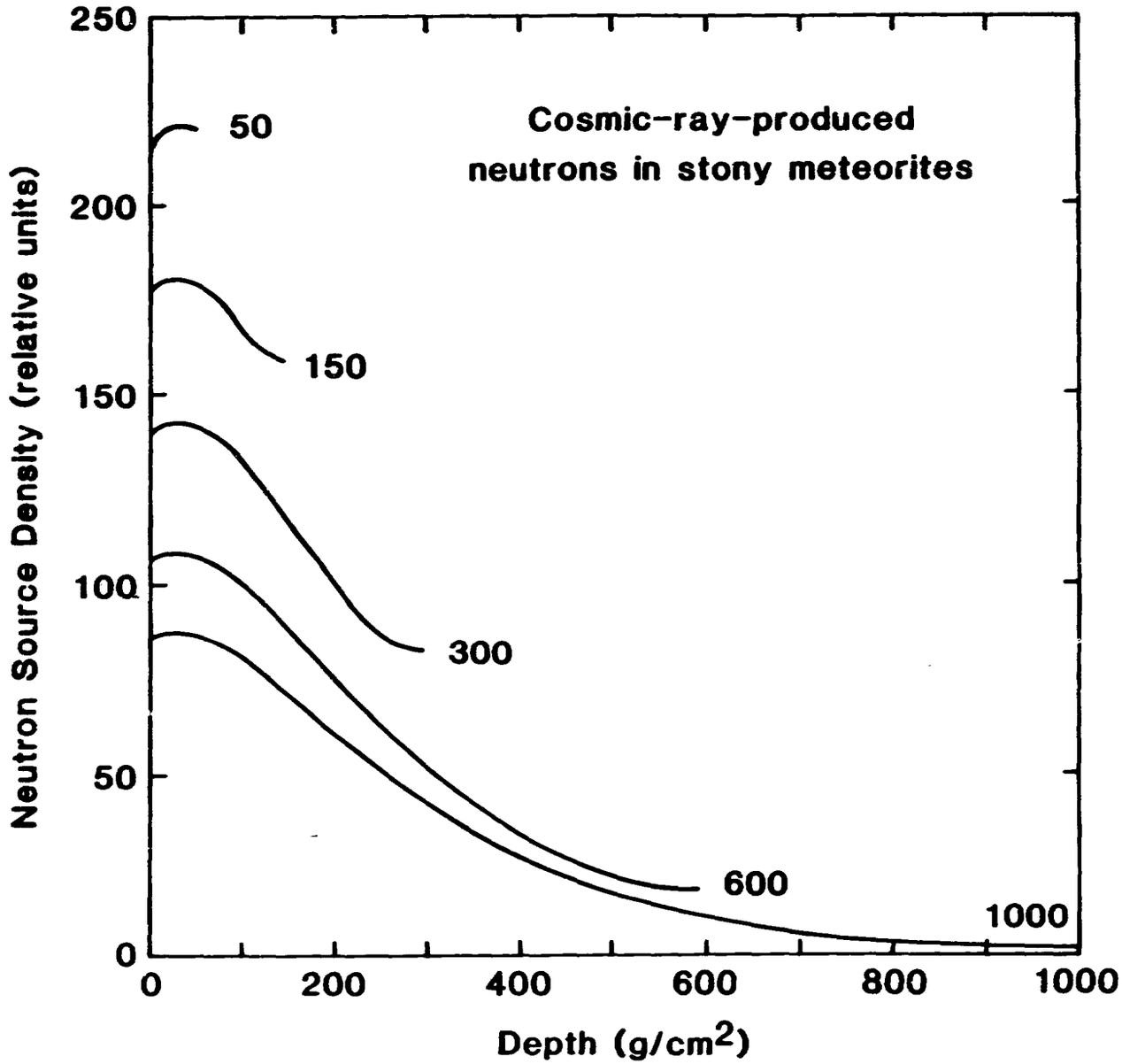
Cosmic-ray-produced
neutrons in stony meteorites
Neutron Source Density (relative units)
Depth (g/cm2)
250
200
150
100
50
0
0
200
400
600
800
1000
50
150
300
600
1000

Fig. 1.

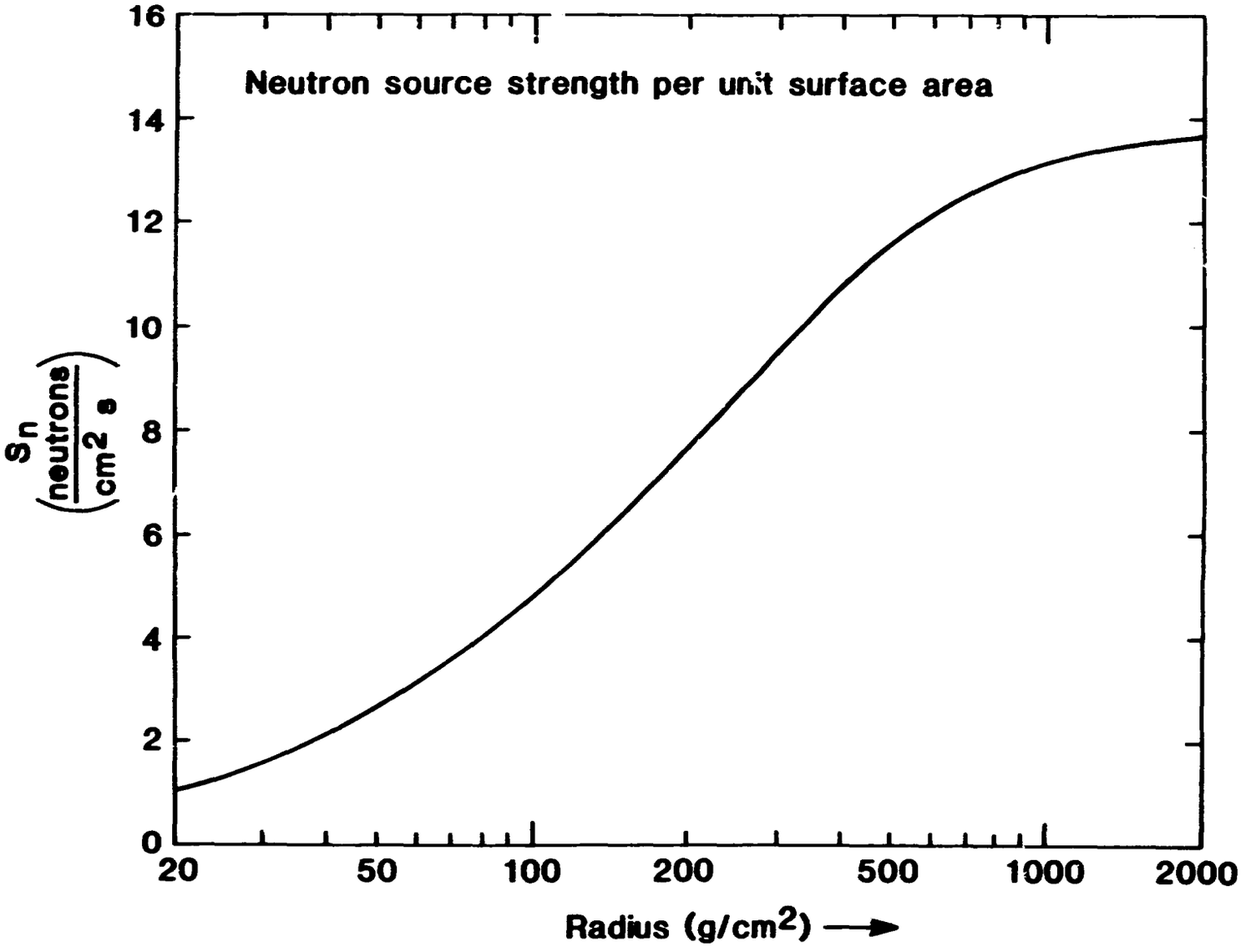
Neutron source strength per unit surface area
$S_n \left(\frac{\text{neutrons}}{\text{cm}^2\ \text{s}}\right)$
0
2
4
6
8
10
12
14
16
20
50
100
200
500
1000
2000
Radius (g/cm^2) ⟶

Fig. 2.

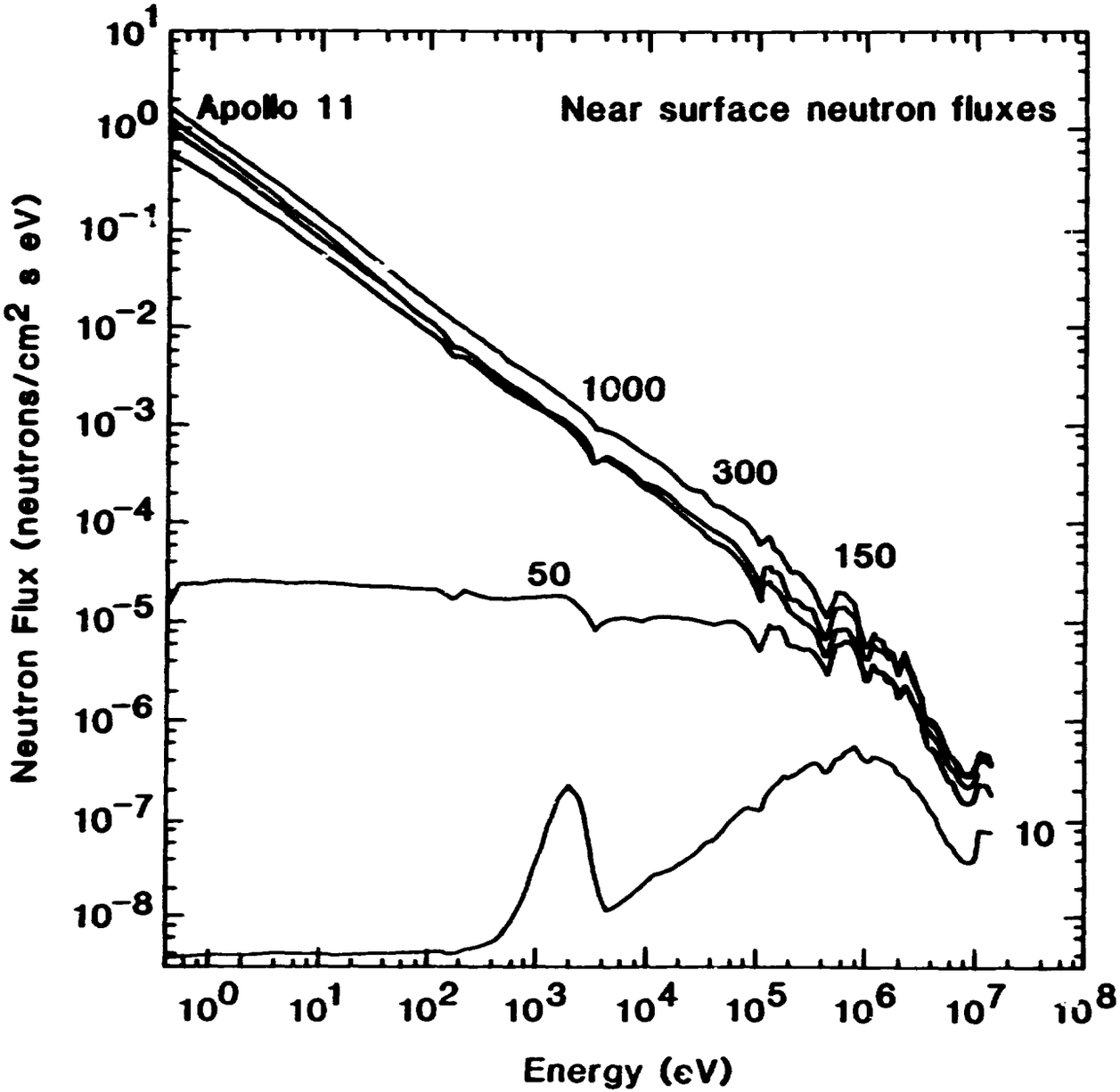
Apollo 11
Near surface neutron fluxes
Neutron Flux (neutrons/cm² s eV)
Energy (eV)
1000
300
150
50
10

Fig. 3.

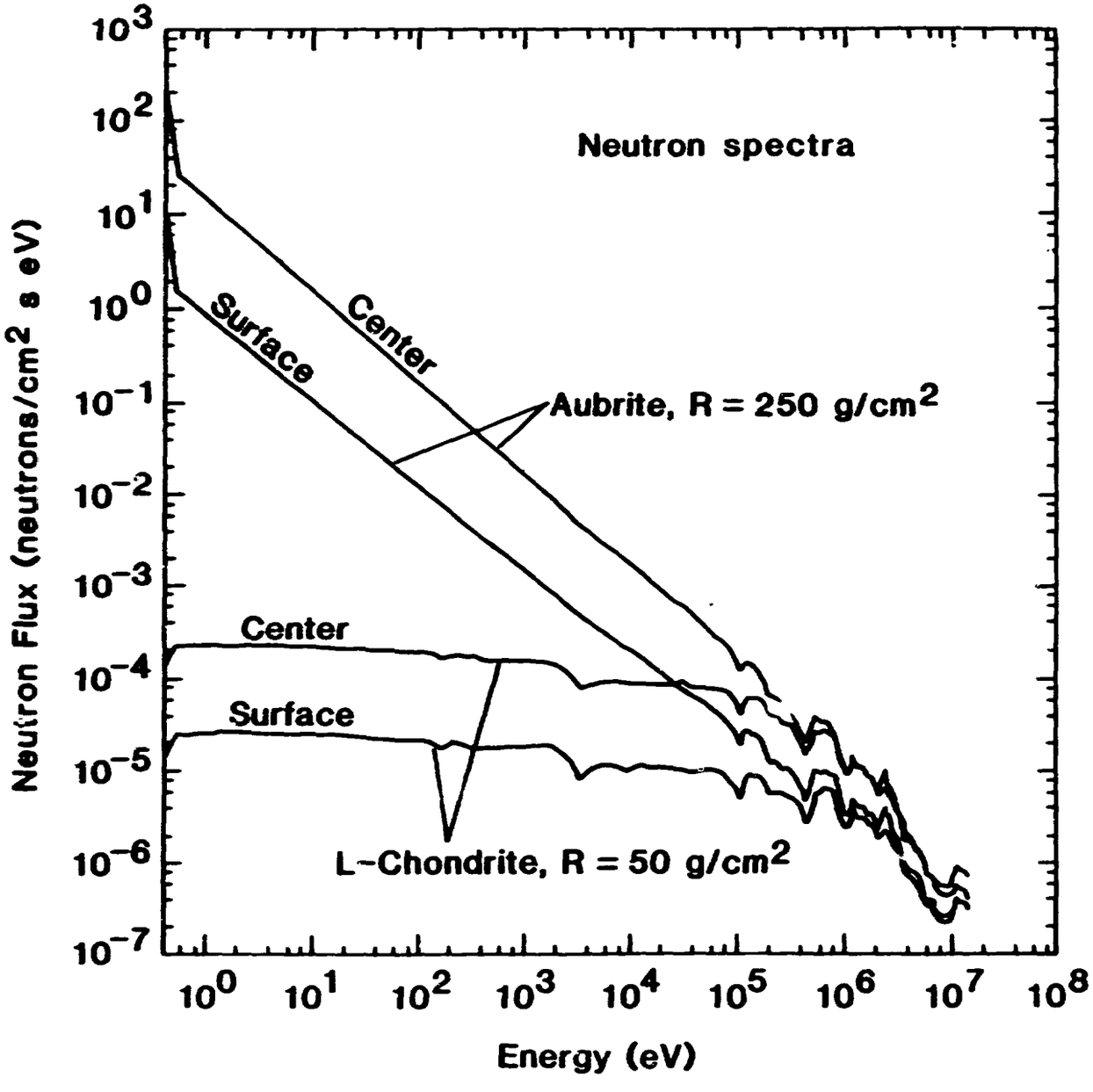
Neutron spectra
Center
Surface
Aubrite, R = 250 g/cm2
Center
Surface
L-Chondrite, R = 50 g/cm2
Neutron Flux (neutrons/cm2 s eV)
Energy (eV)
10^3
10^2
10^1
10^0
10^-1
10^-2
10^-3
10^-4
10^-5
10^-6
10^-7
10^0 10^1 10^2 10^3 10^4 10^5 10^6 10^7 10^8

Fig. 4.

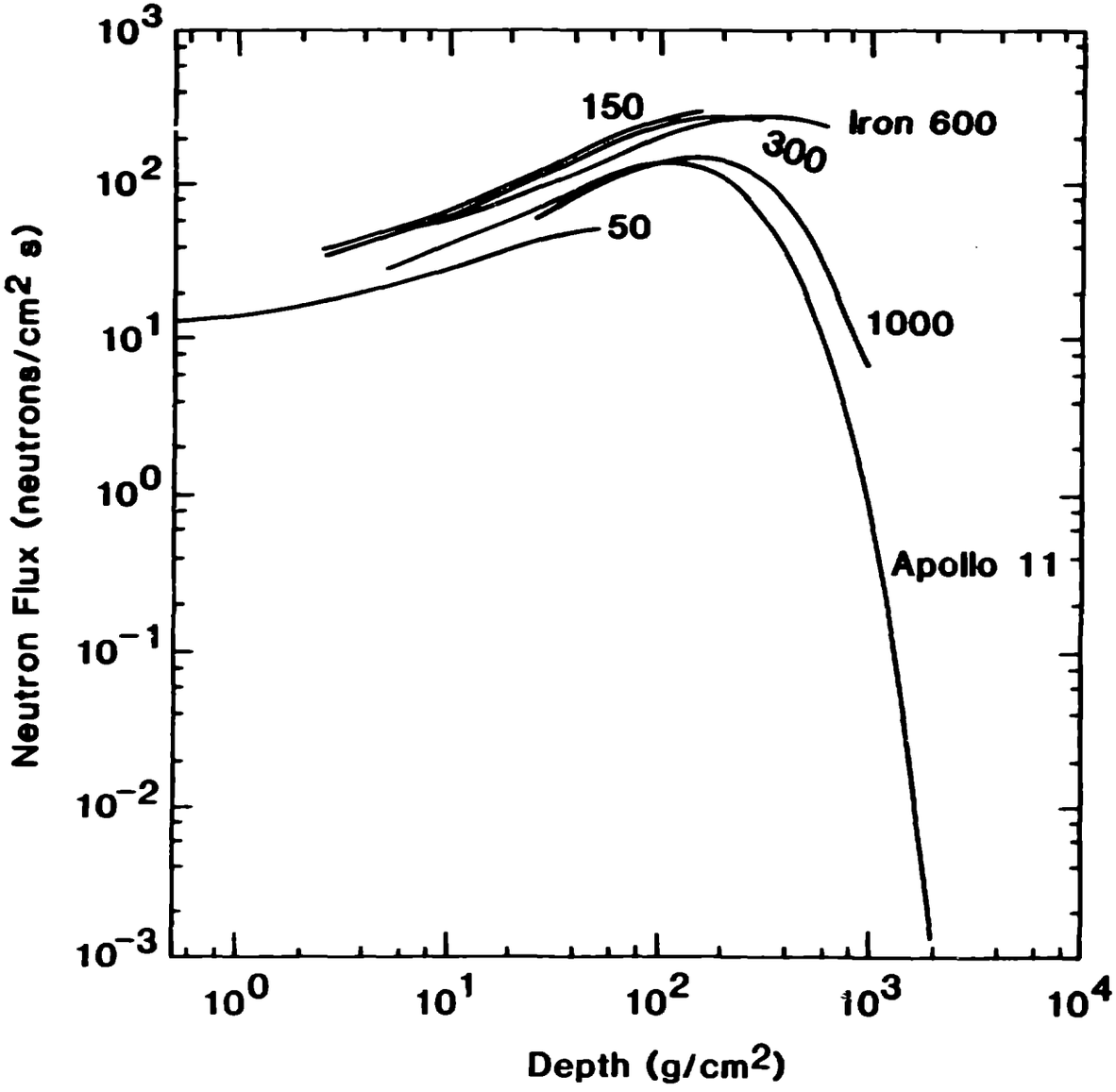
Neutron Flux (neutrons/cm^2 s)
10^3
10^2
10^1
10^0
10^{-1}
10^{-2}
10^{-3}
150
Iron 600
300
50
1000
Apollo 11
10^0
10^1
10^2
10^3
10^4
Depth (g/cm^2)

Fig. 5.

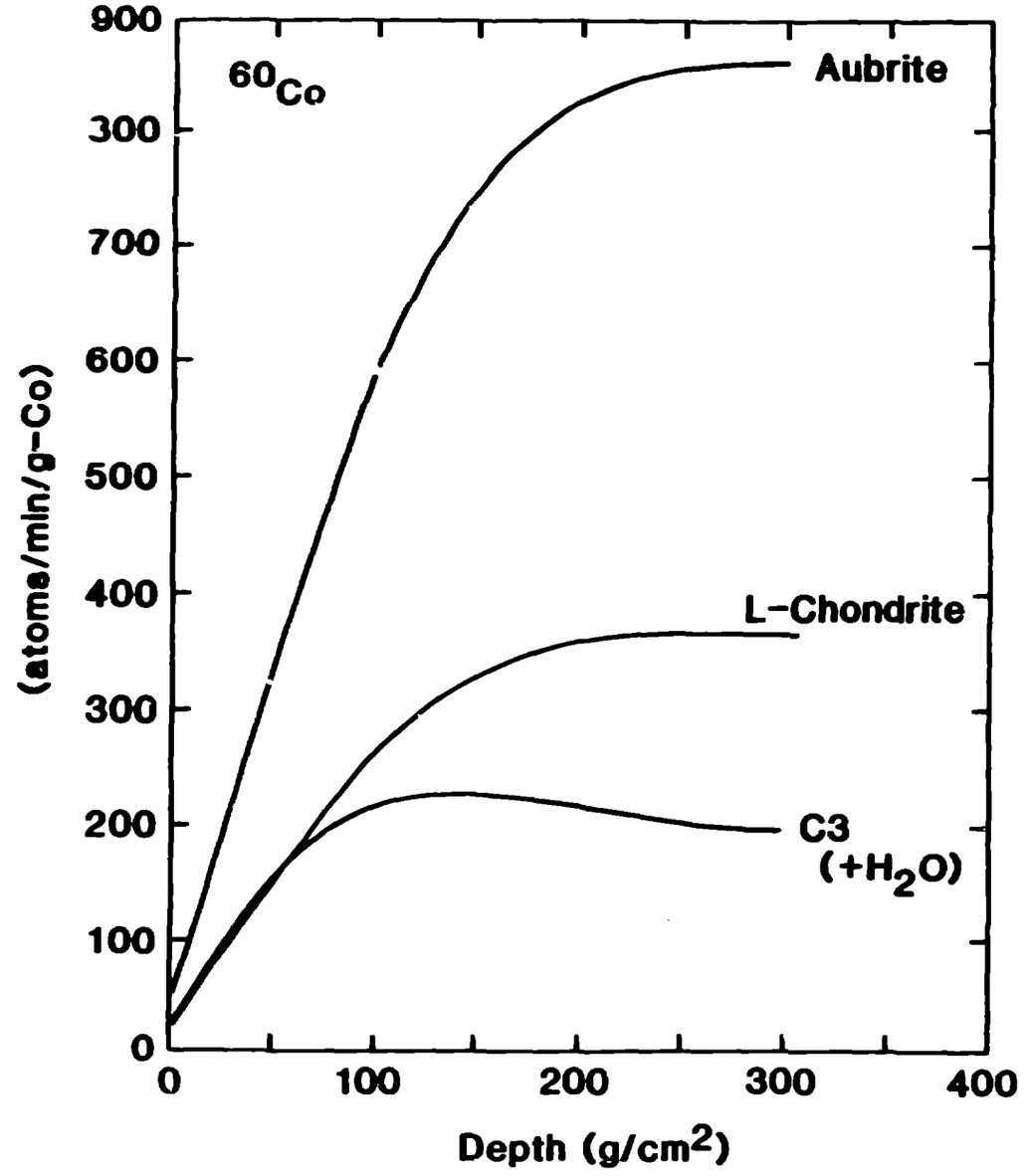
900
300
700
600
500
400
300
200
100
0
0
100
200
300
400
^{60}Co
Aubrite
L-Chondrite
C3
(+H_2O)
(atoms/min/g-Co)
Depth (g/cm^2)

Fig. 6.

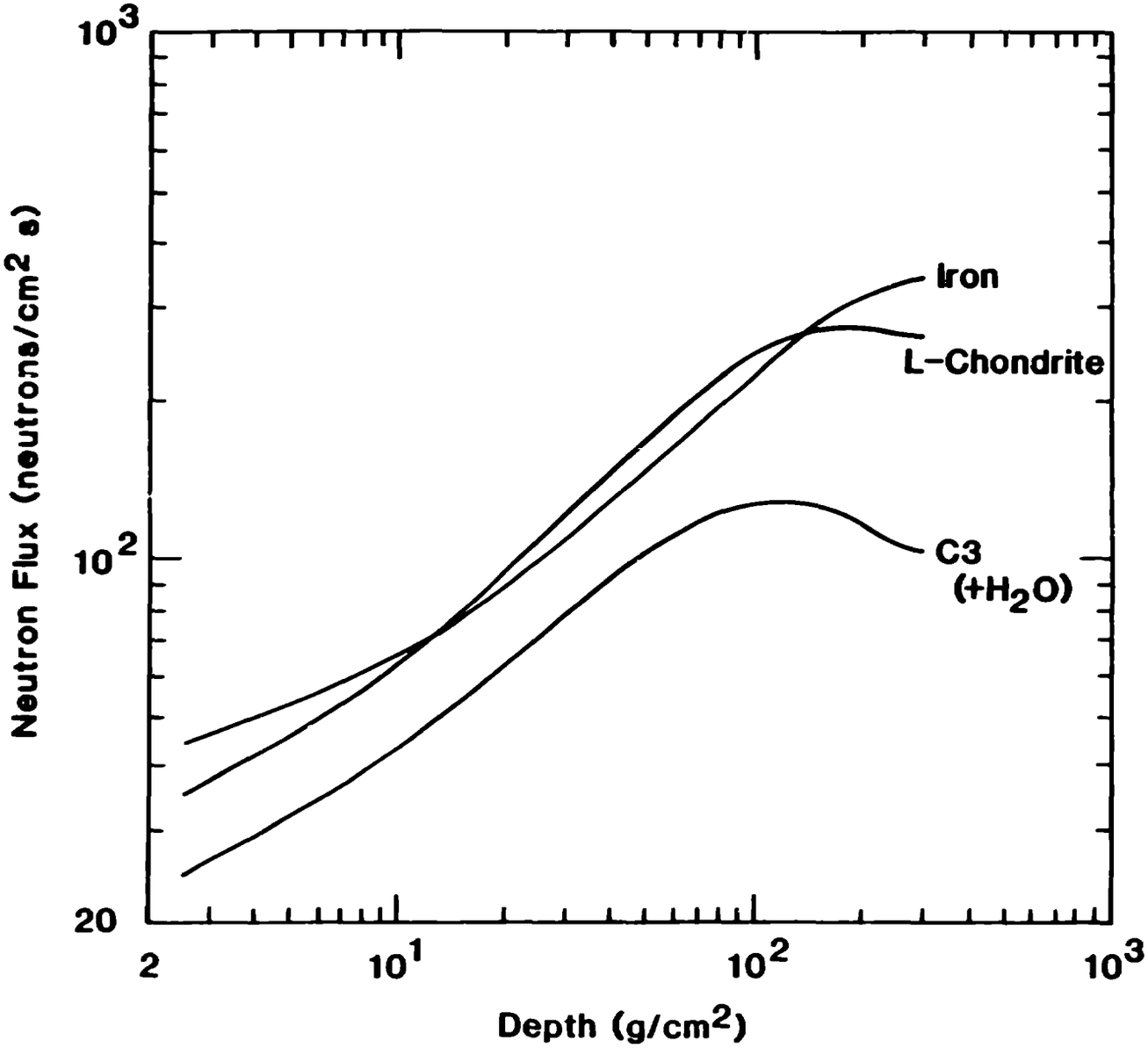
10^3
10^2
20
2
10^1
10^2
10^3
Neutron Flux (neutrons/cm^2 s)
Depth (g/cm^2)
Iron
L-Chondrite
C3
(+H_2O)

Fig. 7.

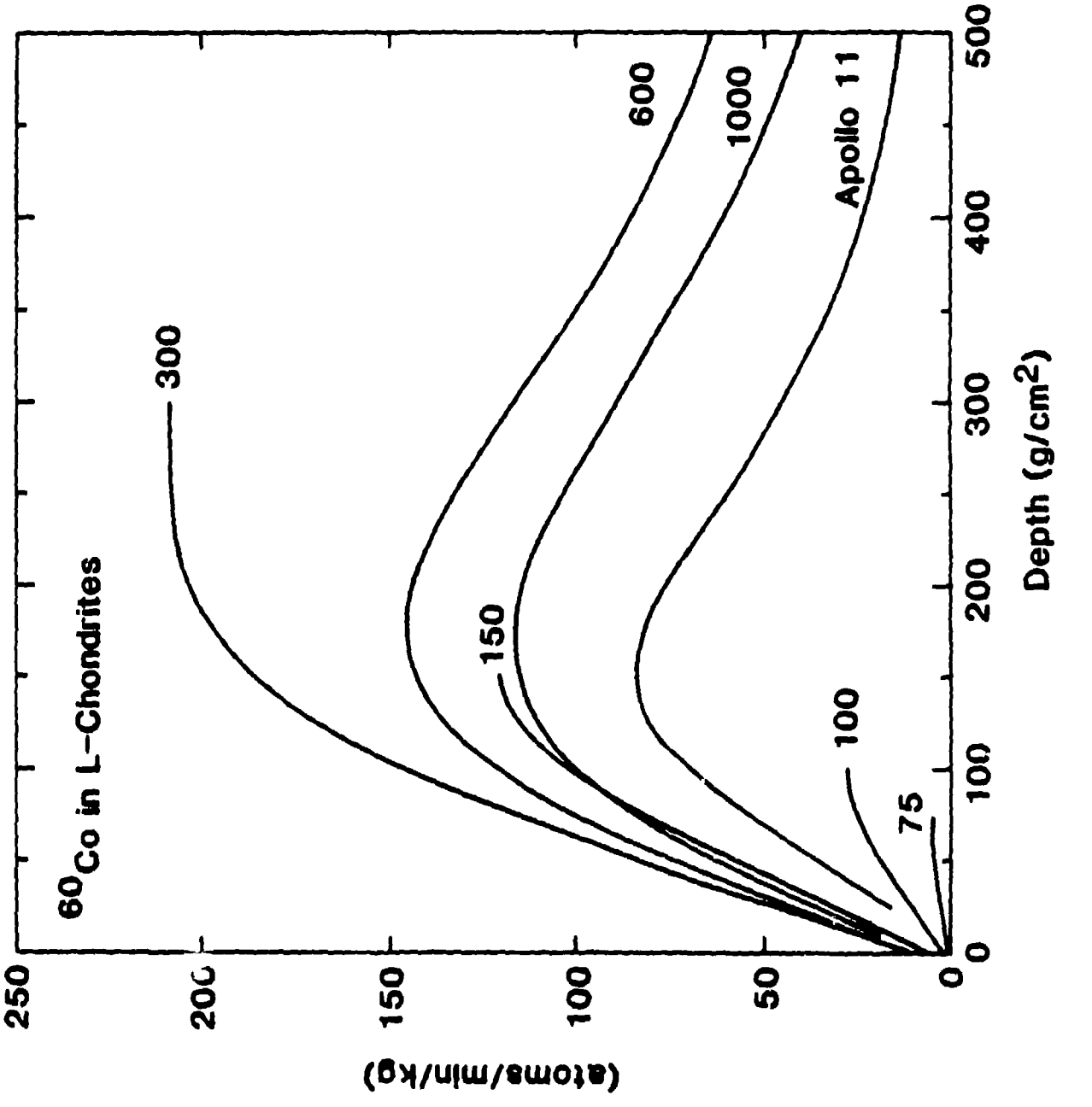
^{60}Co in L-Chondrites
(atoms/min/kg)
250
200
150
100
50
0
Depth (g/cm^2)
0
100
200
300
400
500
75
100
150
300
600
1000
Apollo 11

Fig. 8.

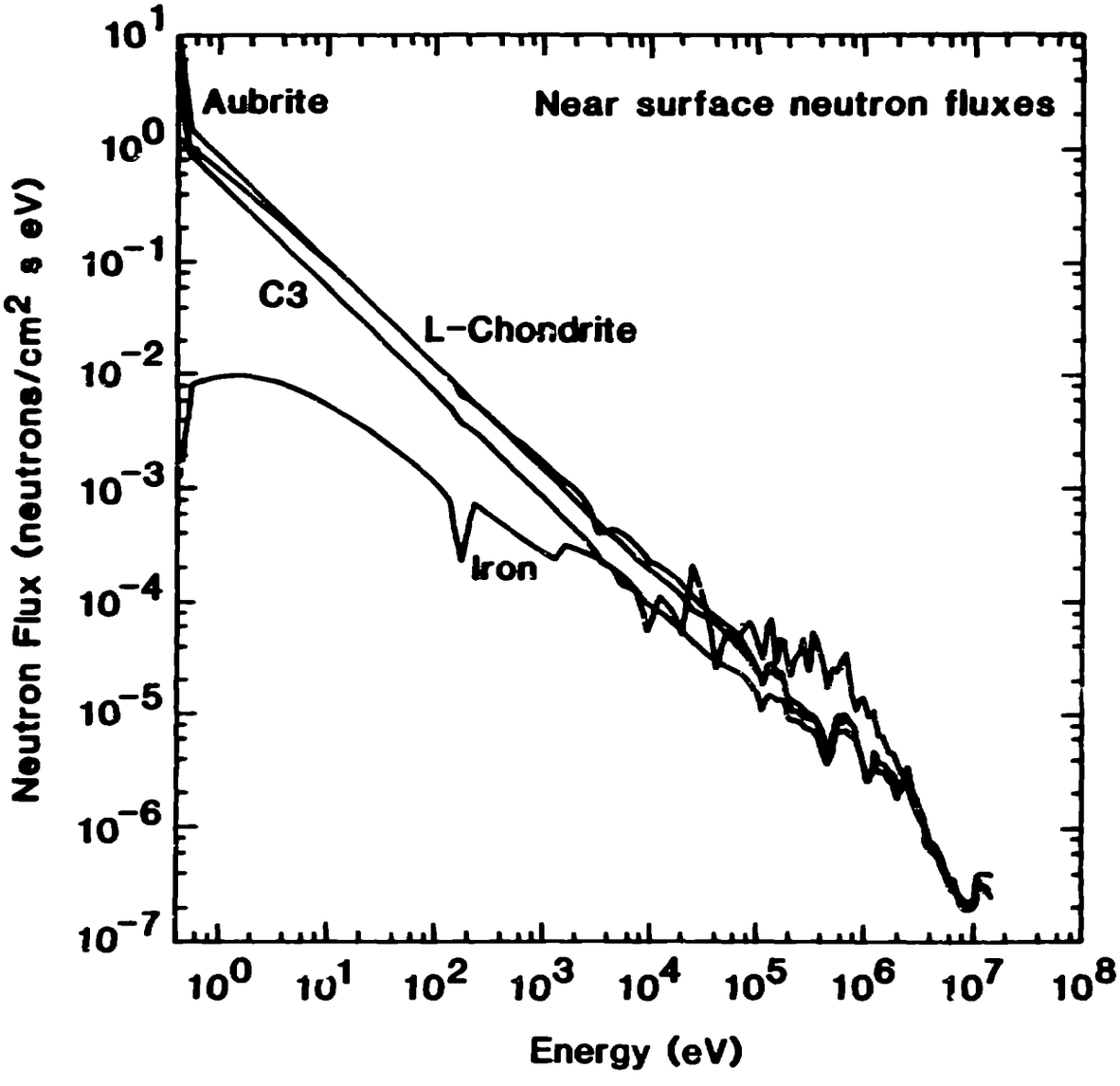
Near surface neutron fluxes
Aubrite
C3
L-Chondrite
Iron
Neutron Flux (neutrons/cm² s eV)
Energy (eV)
10¹
10⁰
10⁻¹
10⁻²
10⁻³
10⁻⁴
10⁻⁵
10⁻⁶
10⁻⁷
10⁰ 10¹ 10² 10³ 10⁴ 10⁵ 10⁶ 10⁷ 10⁸

Fig. 9.

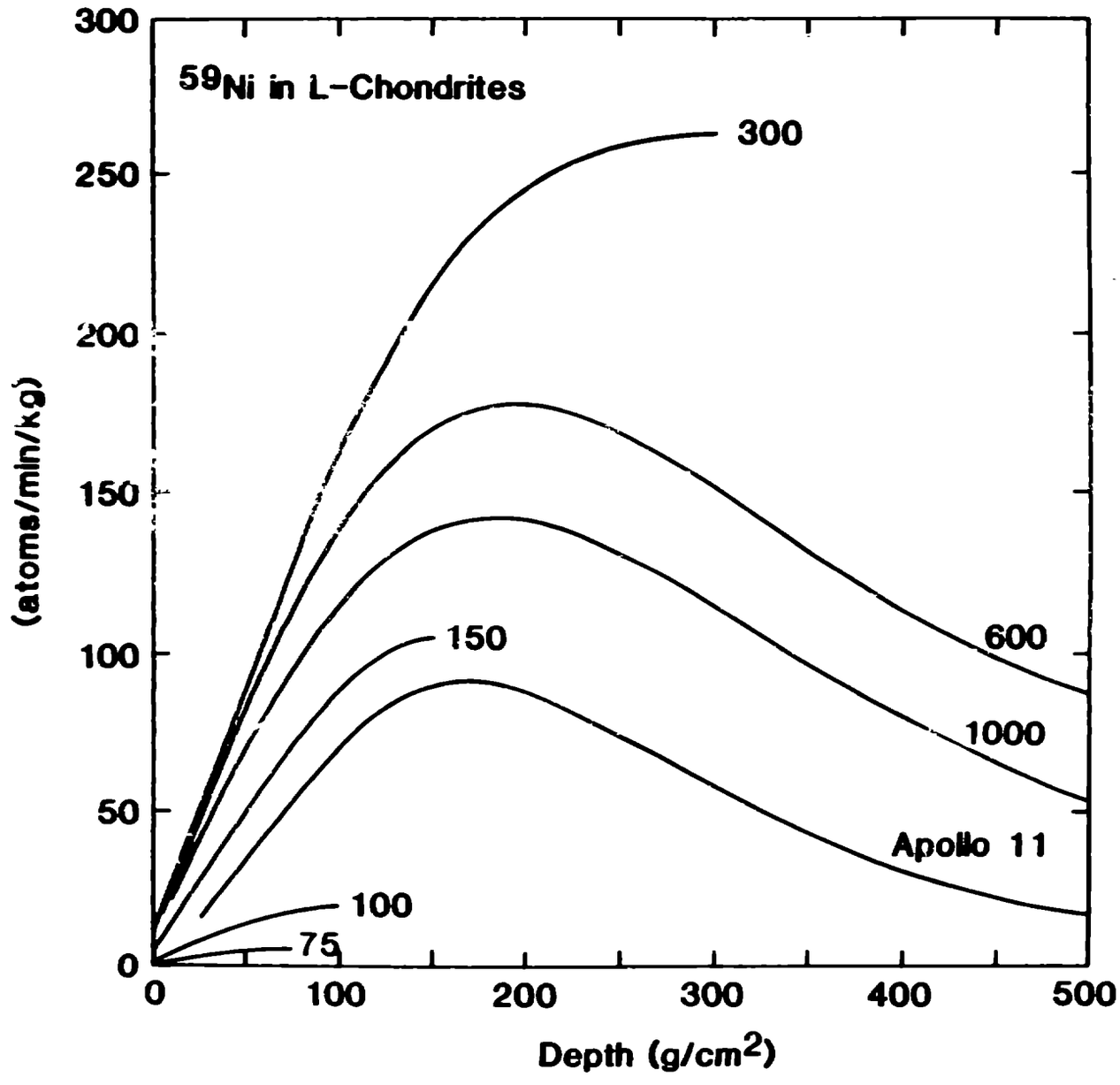
59Ni in L-Chondrites
300
250
200
150
100
50
0
(atoms/min/kg)
300
600
1000
Apollo 11
150
100
75
0
100
200
300
400
500
Depth (g/cm2)

Fig. 10.

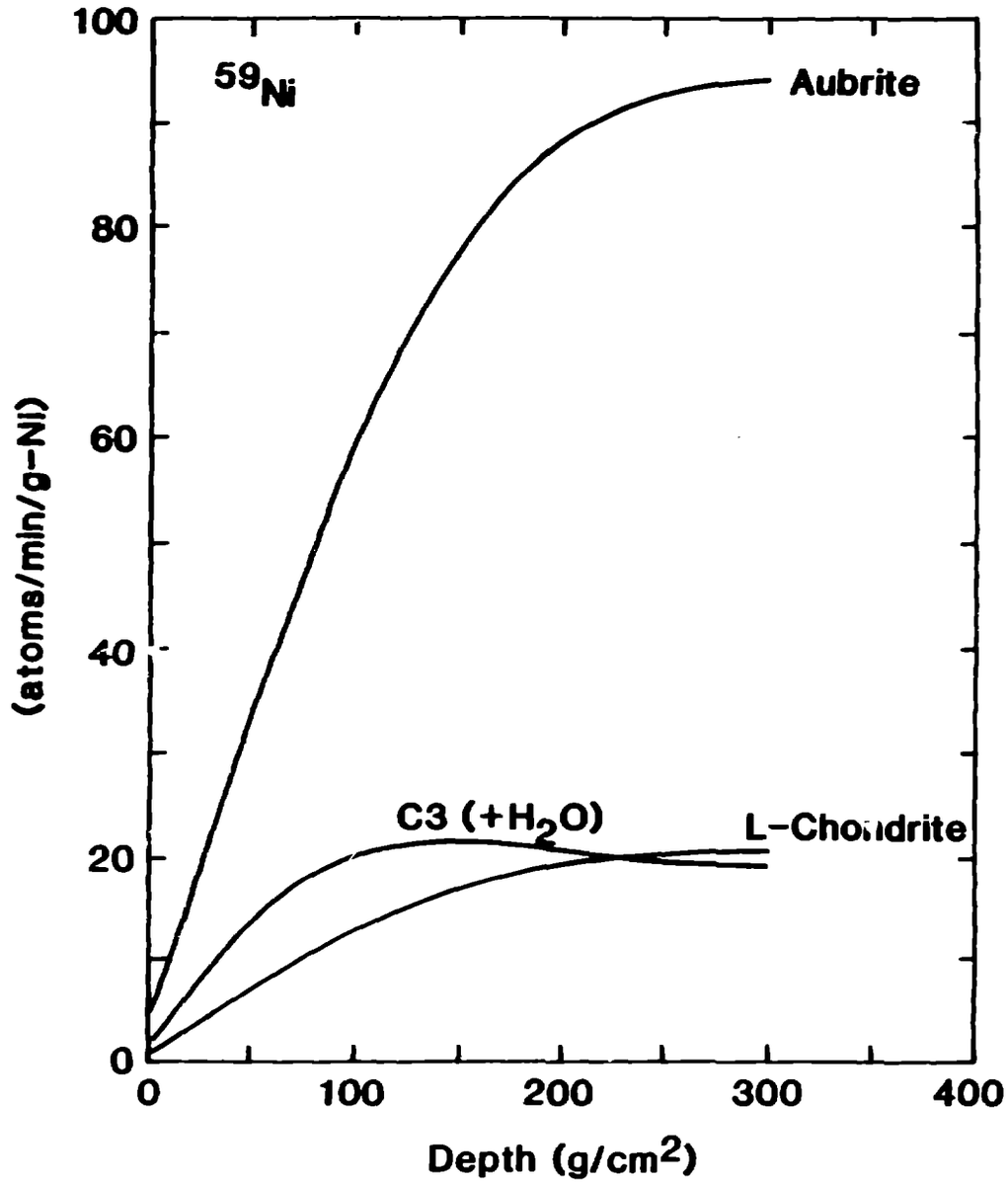
100
80
60
40
20
0
0
100
200
300
400
^{59}Ni
Aubrite
C3 (+H_2O)
L-Chondrite
(atoms/min/g-Ni)
Depth (g/cm^2)

Fig. 11.

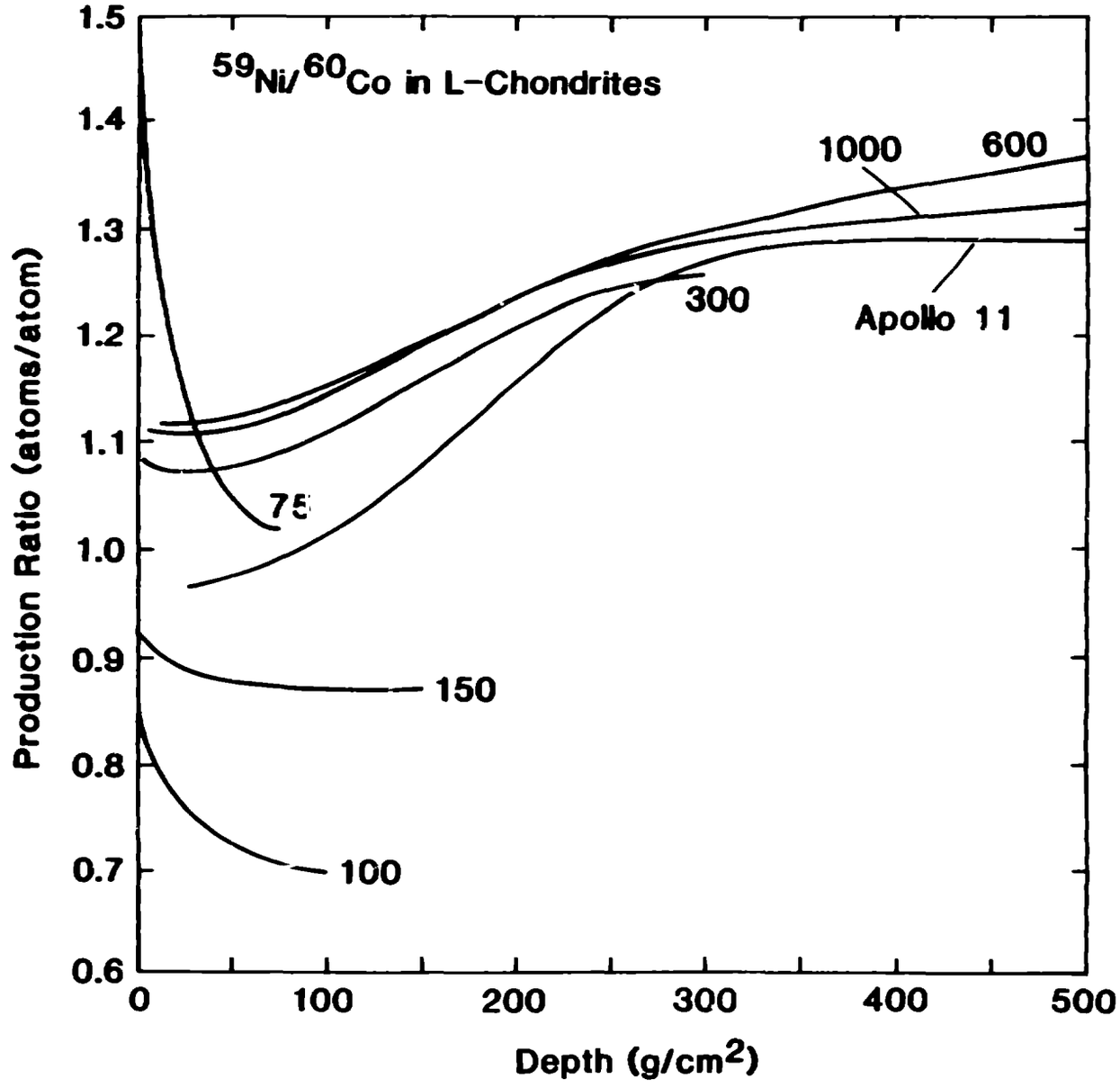
$^{59}Ni/^{60}Co$ in L-Chondrites
Production Ratio (atoms/atom)
Depth (g/cm^2)
1.5
1.4
1.3
1.2
1.1
1.0
0.9
0.8
0.7
0.6
0
100
200
300
400
500
1000
600
300
Apollo 11
75
150
100

Fig. 12.

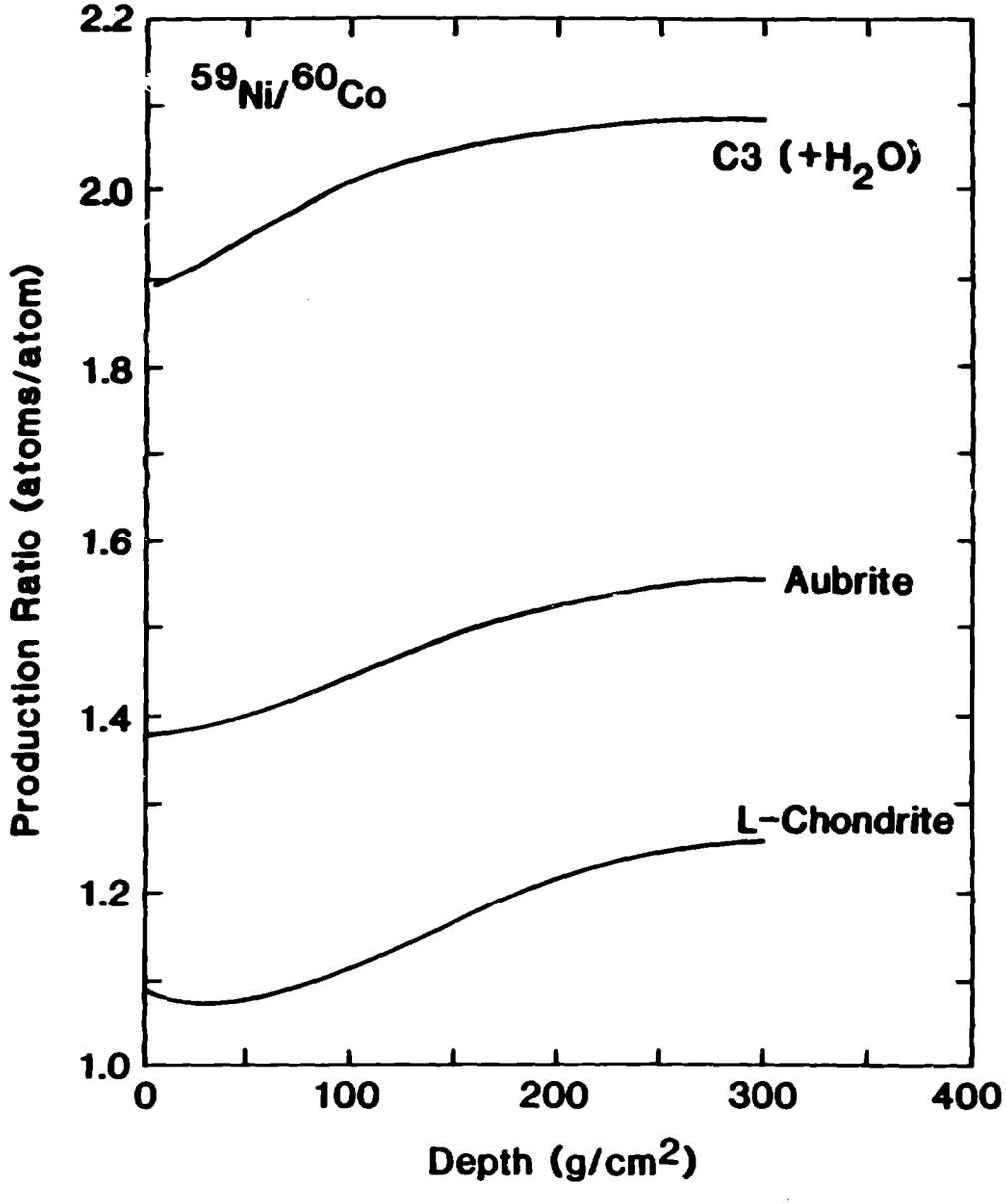
$^{59}Ni/^{60}Co$
C3 (+H_2O)
Aubrite
L-Chondrite
Production Ratio (atoms/atom)
Depth (g/cm^2)
2.2
2.0
1.8
1.6
1.4
1.2
1.0
0
100
200
300
400

Fig. 13.

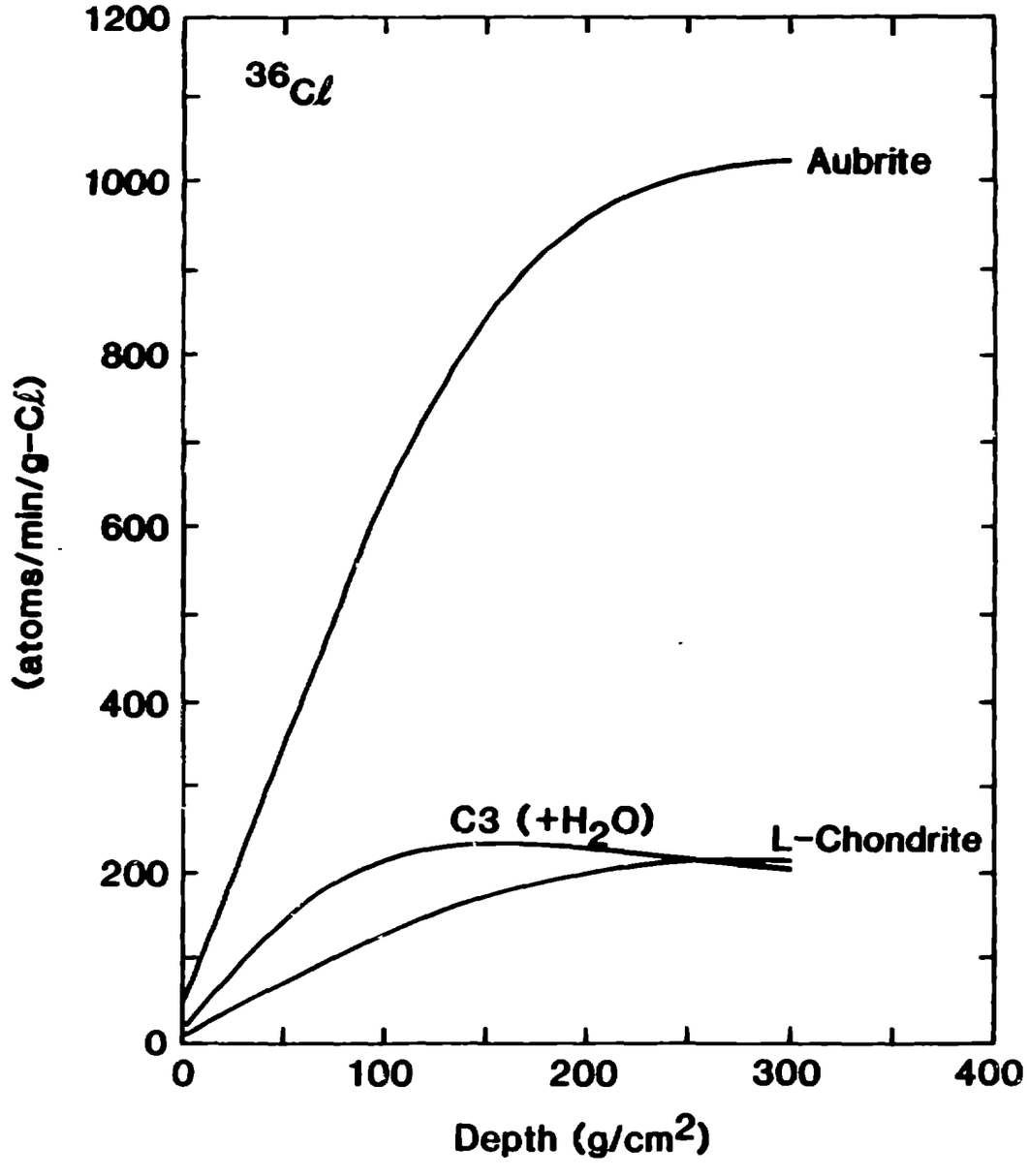
1200
1000
800
600
400
200
0
^{36}Cl
Aubrite
C3 (+H_2O)
L-Chondrite
(atoms/min/g-Cl)
0
100
200
300
400
Depth (g/cm^2)

Fig. 14.

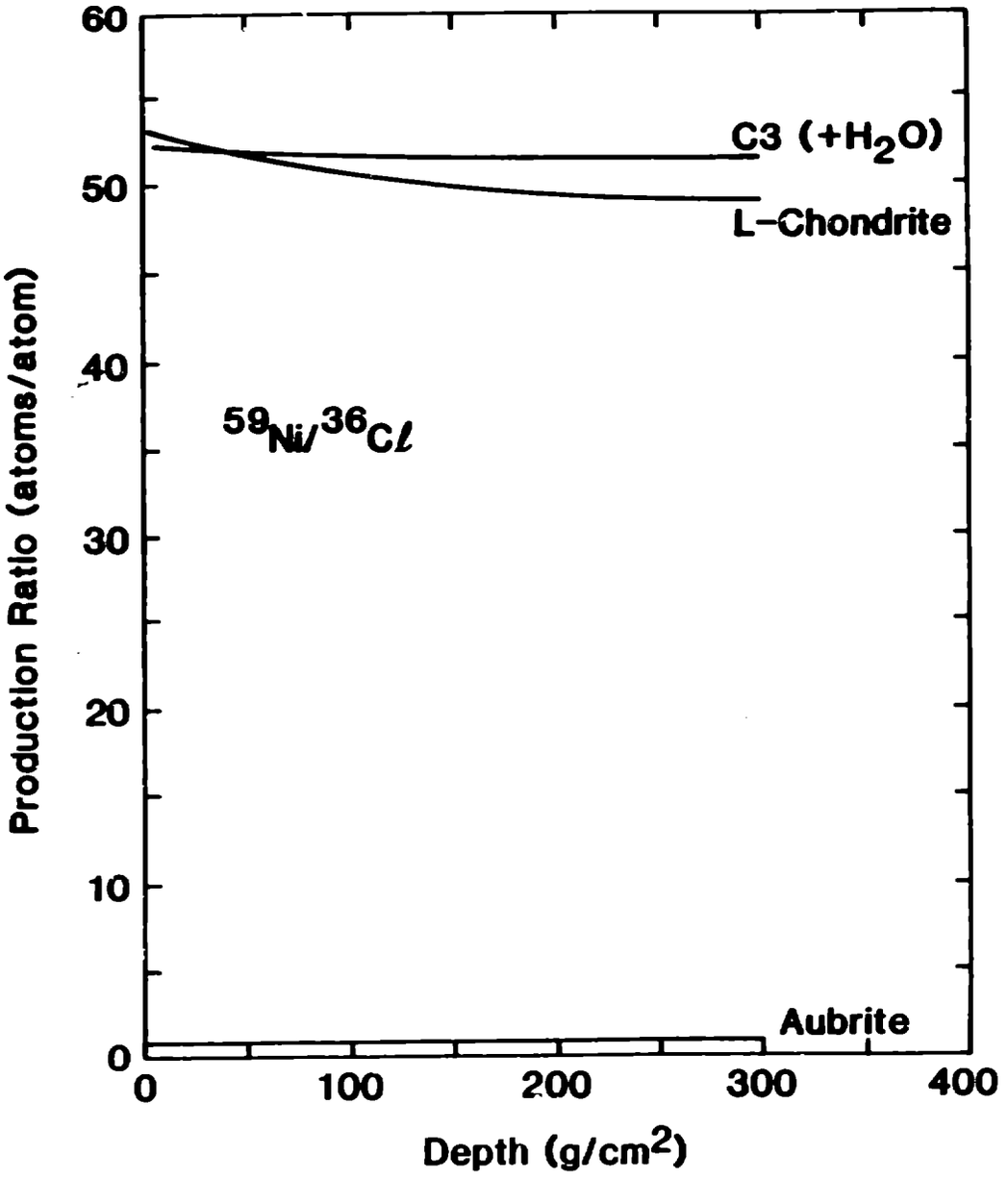
60
50
40
30
20
10
0
Production Ratio (atoms/atom)
C3 (+H2O)
L-Chondrite
59Ni/36Cl
Aubrite
0
100
200
300
400
Depth (g/cm2)

Fig. 15.